

The Efficient Generation of Laboratory Waves

Correct to Second-order

by

Brian W. Giesbrecht

A Thesis

Submitted to the Faculty of Graduate Studies

in Partial Fulfillment of the Requirements

for the Degree of

Master of Science

Department of Civil and Geological Engineering

University of Manitoba

Winnipeg, Manitoba

© December, 1996



National Library
of Canada

Acquisitions and
Bibliographic Services Branch

395 Wellington Street
Ottawa, Ontario
K1A 0N4

Bibliothèque nationale
du Canada

Direction des acquisitions et
des services bibliographiques

395, rue Wellington
Ottawa (Ontario)
K1A 0N4

Your file *Votre référence*

Our file *Notre référence*

The author has granted an irrevocable non-exclusive licence allowing the National Library of Canada to reproduce, loan, distribute or sell copies of his/her thesis by any means and in any form or format, making this thesis available to interested persons.

L'auteur a accordé une licence irrévocable et non exclusive permettant à la Bibliothèque nationale du Canada de reproduire, prêter, distribuer ou vendre des copies de sa thèse de quelque manière et sous quelque forme que ce soit pour mettre des exemplaires de cette thèse à la disposition des personnes intéressées.

The author retains ownership of the copyright in his/her thesis. Neither the thesis nor substantial extracts from it may be printed or otherwise reproduced without his/her permission.

L'auteur conserve la propriété du droit d'auteur qui protège sa thèse. Ni la thèse ni des extraits substantiels de celle-ci ne doivent être imprimés ou autrement reproduits sans son autorisation.

ISBN 0-612-16140-4

Canada

Name Brian W. Giesbrecht

Dissertation Abstracts International and Masters Abstracts International are arranged by broad, general subject categories. Please select the one subject which most nearly describes the content of your dissertation or thesis. Enter the corresponding four-digit code in the spaces provided.

SUBJECT TERM

Civil Engineering

0543

UMI

SUBJECT CODE

Subject Categories

THE HUMANITIES AND SOCIAL SCIENCES

COMMUNICATIONS AND THE ARTS

Architecture 0729
 Art History 0377
 Cinema 0900
 Dance 0378
 Design and Decorative Arts 0389
 Fine Arts 0357
 Information Science 0723
 Journalism 0391
 Landscape Architecture 0390
 Library Science 0399
 Mass Communications 0708
 Music 0413
 Speech Communication 0459
 Theater 0465

EDUCATION

General 0515
 Administration 0514
 Adult and Continuing 0516
 Agricultural 0517
 Art 0273
 Bilingual and Multicultural 0282
 Business 0688
 Community College 0275
 Curriculum and Instruction 0727
 Early Childhood 0518
 Elementary 0524
 Educational Psychology 0525
 Finance 0277
 Guidance and Counseling 0519
 Health 0680
 Higher 0745
 History of 0520
 Home Economics 0278
 Industrial 0521
 Language and Literature 0279
 Mathematics 0280
 Music 0522
 Philosophy of 0998

Physical 0523
 Reading 0535
 Religious 0527
 Sciences 0714
 Secondary 0533
 Social Sciences 0534
 Sociology of 0340
 Special 0529
 Teacher Training 0530
 Technology 0710
 Tests and Measurements 0288
 Vocational 0747

LANGUAGE, LITERATURE AND LINGUISTICS

Language
 General 0679
 Ancient 0289
 Linguistics 0290
 Modern 0291
 Rhetoric and Composition 0681
 Literature
 General 0401
 Classical 0294
 Comparative 0295
 Medieval 0297
 Modern 0298
 African 0316
 American 0591
 Asian 0305
 Canadian (English) 0352
 Canadian (French) 0355
 Caribbean 0360
 English 0593
 Germanic 0311
 Latin American 0312
 Middle Eastern 0315
 Romance 0313
 Slavic and East European 0314

PHILOSOPHY, RELIGION AND THEOLOGY

Philosophy 0422
 Religion
 General 0318
 Biblical Studies 0321
 Clergy 0319
 History of 0320
 Philosophy of 0322
 Theology 0469

SOCIAL SCIENCES

American Studies 0323
 Anthropology
 Archaeology 0324
 Cultural 0326
 Physical 0327
 Business Administration
 General 0310
 Accounting 0272
 Banking 0770
 Management 0454
 Marketing 0338
 Canadian Studies 0385
 Economics
 General 0501
 Agricultural 0503
 Commerce-Business 0505
 Finance 0508
 History 0509
 Labor 0510
 Theory 0511
 Folklore 0358
 Geography 0366
 Gerontology 0351
 History
 General 0578
 Ancient 0579

Medieval 0581
 Modern 0582
 Church 0330
 Black 0328
 African 0331
 Asia, Australia and Oceania 0332
 Canadian 0334
 European 0335
 Latin American 0336
 Middle Eastern 0333
 United States 0337
 History of Science 0585
 Law 0398
 Political Science
 General 0615
 International Law and Relations 0616
 Public Administration 0617
 Recreation 0814
 Social Work 0452
 Sociology
 General 0626
 Criminology and Penology 0627
 Demography 0938
 Ethnic and Racial Studies 0631
 Individual and Family Studies 0628
 Industrial and Labor Relations 0629
 Public and Social Welfare 0630
 Social Structure and Development 0700
 Theory and Methods 0344
 Transportation 0709
 Urban and Regional Planning 0999
 Women's Studies 0453

THE SCIENCES AND ENGINEERING

BIOLOGICAL SCIENCES

Agriculture
 General 0473
 Agronomy 0285
 Animal Culture and Nutrition 0475
 Animal Pathology 0476
 Fisheries and Aquaculture 0792
 Food Science and Technology 0359
 Forestry and Wildlife 0478
 Plant Culture 0479
 Plant Pathology 0480
 Range Management 0777
 Soil Science 0481
 Wood Technology 0746
 Biology
 General 0306
 Anatomy 0287
 Animal Physiology 0433
 Biostatistics 0308
 Botany 0309
 Cell 0379
 Ecology 0329
 Entomology 0353
 Genetics 0369
 Limnology 0793
 Microbiology 0410
 Molecular 0307
 Neuroscience 0317
 Oceanography 0416
 Plant Physiology 0817
 Veterinary Science 0778
 Zoology 0472
 Biophysics
 General 0786
 Medical 0760

Geodesy 0370
 Geology 0372
 Geophysics 0373
 Hydrology 0388
 Mineralogy 0411
 Paleobotany 0345
 Paleoecology 0426
 Paleontology 0418
 Paleozoology 0985
 Palynology 0427
 Physical Geography 0368
 Physical Oceanography 0415

HEALTH AND ENVIRONMENTAL SCIENCES

Environmental Sciences 0768
 Health Sciences
 General 0566
 Audiology 0300
 Dentistry 0567
 Education 0350
 Administration, Health Care 0769
 Human Development 0758
 Immunology 0982
 Medicine and Surgery 0564
 Mental Health 0347
 Nursing 0569
 Nutrition 0570
 Obstetrics and Gynecology 0380
 Occupational Health and Safety 0354
 Oncology 0992
 Ophthalmology 0381
 Pathology 0571
 Pharmacology 0419
 Pharmacy 0572
 Public Health 0573
 Radiology 0574
 Recreation 0575
 Rehabilitation and Therapy 0382

Speech Pathology 0460
 Toxicology 0383
 Home Economics 0386

PHYSICAL SCIENCES

Pure Sciences
 Chemistry
 General 0485
 Agricultural 0749
 Analytical 0486
 Biochemistry 0487
 Inorganic 0488
 Nuclear 0738
 Organic 0490
 Pharmaceutical 0491
 Physical 0494
 Polymer 0495
 Radiation 0754
 Mathematics 0405
 Physics
 General 0605
 Acoustics 0986
 Astronomy and Astrophysics 0606
 Atmospheric Science 0608
 Atomic 0748
 Condensed Matter 0611
 Electricity and Magnetism 0607
 Elementary Particles and High Energy 0798
 Fluid and Plasma 0759
 Molecular 0609
 Nuclear 0610
 Optics 0752
 Radiation 0756
 Statistics 0463
 Applied Sciences
 Applied Mechanics 0346
 Computer Science 0984

Engineering
 General 0537
 Aerospace 0538
 Agricultural 0539
 Automotive 0540
 Biomedical 0541
 Chemical 0542
 Civil 0543
 Electronics and Electrical 0544
 Environmental 0775
 Industrial 0546
 Marine and Ocean 0547
 Materials Science 0794
 Mechanical 0548
 Metallurgy 0743
 Mining 0551
 Nuclear 0552
 Packaging 0549
 Petroleum 0765
 Sanitary and Municipal 0554
 System Science 0790
 Geotechnology 0428
 Operations Research 0796
 Plastics Technology 0795
 Textile Technology 0994

PSYCHOLOGY

General 0621
 Behavioral 0384
 Clinical 0622
 Cognitive 0633
 Developmental 0620
 Experimental 0623
 Industrial 0624
 Personality 0625
 Physiological 0989
 Psychobiology 0349
 Psychometrics 0632
 Social 0451

EARTH SCIENCES

Biogeochemistry 0425
 Geochemistry 0996

**THE UNIVERSITY OF MANITOBA
FACULTY OF GRADUATE STUDIES
COPYRIGHT PERMISSION**

**THE EFFICIENT GERNATION OF LABORATORY WAVES CORRECT
TO SECOND-ORDER**

BY

BRIAN W. GIESBRECHT

**A Thesis/Practicum submitted to the Faculty of Graduate Studies of the University of Manitoba in partial
fulfillment of the requirements for the degree of**

MASTER OF SCIENCE

Brian W. Giesbrecht © 1996

**Permission has been granted to the LIBRARY OF THE UNIVERSITY OF MANITOBA to lend or sell copies
of this thesis/practicum, to the NATIONAL LIBRARY OF CANADA to microfilm this thesis/practicum and
to lend or sell copies of the film, and to UNIVERSITY MICROFILMS INC. to publish an abstract of this
thesis/practicum..**

**This reproduction or copy of this thesis has been made available by authority of the copyright owner solely
for the purpose of private study and research, and may only be reproduced and copied as permitted by
copyright laws or with express written authorization from the copyright owner.**

Table of Contents

Table of Contents	ii
List of Figures	iv
Abstract.....	vi
List of Symbols and Notation.....	vii
Acknowledgments	xi
Chapter 1: Introduction	
1.1. Background.....	1
1.2. Literature Review.....	1
1.3. Objectives of this Research.....	6
Chapter 2: Wavemaker Theory	
2.1. Governing Equations.....	8
2.2. First-Order Solution	12
2.3. Second-Order Solution : Long Waves	13
2.4. Second-Order Solution : Short Waves.....	24
Chapter 3: Wave Generation Software	
3.1. General Overview.....	34
3.2. First-Order Wave Generation	36
3.3. Threshold Limited Approach.....	42
3.4. Long Wave Correction.....	43
3.5. Short Wave Correction.....	49

3.6. Driving Signal Creation	55
Chapter 4: Physical Testing	
4.1. Apparatus.....	57
4.2. Laboratory Limitations	61
4.2.1. Waveboard Response.....	62
4.2.2. Wave Attenuation.....	65
4.2.3. Wave Reflection	68
Chapter 5: Bispectral Analysis	72
Chapter 6: Conclusions and Recommendations	
6.1. Summary and Conclusions.....	85
6.2. Recommendations For Future Work.....	89
References.....	91

List of Figures

		Page
Figure 2.1	Waveboard definition sketch	10
Figure 2.2	Long wave transfer function G_{nm}^-h as a function of h/L_0	18
Figure 2.3	Long wave transfer function $F_{11}h$ as a function of h/L_0	21
Figure 2.4	Long wave transfer function $F_{12}h$ as a function of h/L_0	22
Figure 2.5	Long wave transfer function F_1h as a function of h/L_0	23
Figure 2.6	Short wave transfer function G_{nm}^+h as a function of h/L_0	26
Figure 2.7	Short wave transfer function F_1h as a function of h/L_0	30
Figure 2.8	Short wave transfer function $F_{23}h$ as a function of h/L_0	32
Figure 3.1	LINWAVE first-order wave generation algorithm	37
Figure 3.2	Idealized wave spectra used in WAVGEN	40
Figure 3.3	WAVGEN first-order wave generation screen display	41
Figure 3.4	LONGWAVE second-order correction algorithm	44
Figure 3.5	Application of threshold in long wave calculations	45
Figure 3.6	Long wave correction computation times	47
Figure 3.7	Results of various threshold values on calculated long wave	48
Figure 3.8	SHRTWAVE second-order correction algorithm	50
Figure 3.9	Application of threshold in short wave calculations	51
Figure 3.10	Short wave correction computation times	53
Figure 3.11	Results of various threshold values on calculated short wave	54

Figure 3.12	WAVPADL driving signal generator algorithm	56
Figure 4.1	Schematic of HRTF random wave flume	58
Figure 4.2	Beach sand particle size distribution	60
Figure 4.3	Comparison of driving signal and feedback loop signal	63
Figure 4.4	Comparison of target and measured primary wave spectra	64
Figure 4.5a	Wave height attenuation due to sidewall and bottom friction	67
Figure 4.5b	Wave height attenuation ratio at wave probe location	67
Figure 4.6	Wave height attenuation due to gap around waveboard	69
Figure 4.7	Reflection effect on primary waves	70
Figure 5.1	Bispectral results for uncorrected bichromatic wave train	77
Figure 5.2	Bispectral results for long wave corrected bichromatic wave train	79
Figure 5.3	Bispectral results for short wave corrected bichromatic wave train	80
Figure 5.4	Bispectral results for fully corrected bichromatic wave train	82
Figure 5.5	Bispectral results for uncorrected random wave train	83
Figure 5.6	Bispectral results for fully corrected random wave train	84

Abstract

The laboratory setting provides an opportunity to elucidate various aspects of wave related phenomena. However, the mechanical generation of waves by an impervious waveboard results in a number of second-order problems not inherent with wind-generated waves. Since second-order processes play a fundamental role in many wave-related phenomena, the accurate reproduction of "natural" wave conditions is central to meaningful laboratory experiments. Mathematical algorithms exist that eliminate the spurious second-order waves caused by a first-order control signal. These mathematical algorithms were encoded into an interactive software package using MATLAB to create a first-order wave train and correct it for second-order effects based on user-defined inputs. The efficiency of the algorithms was enhanced using a proposed method of thresholding that limits the range of frequencies over which the various corrections are applied. The software package (WAVGEN) was tested in the HRTF random wave flume. The bispectrum was used to examine the ability of the second-order algorithms to eliminate spurious waves. Bichromatic wave trains showed clearly that the algorithms reduced the second-order wave effects. Random wave tests showed similar results albeit less clearly given the broad-banded nature of the random wave spectra.

Symbols and Notation

Symbols

a	wave amplitude (cosine component) [m]
b	wave amplitude (sine component) [m]
$b(f_1, f_2)$	bicoherence estimate
B	first-order velocity potential parameter
$B(f_1, f_2)$	complex bispectral estimate [(units) ³ / Hz ²]
C	first-order velocity potential parameter
D	first-order velocity potential parameter
$E[]$	expected value or average operator
f	wave frequency [Hz]
f_p	peak frequency [Hz]
f_0	Fourier frequency interval [Hz]
f^*	lowest frequency in linear spectrum [Hz]
F_{ij}	second-order transfer function
F	fetch length [m]
g	constant of acceleration due to gravity [m/s ²]
G	evanescent mode transfer function parameter
G_{nm}	second-order transfer function for bounded waves
h	depth of still water [m]
I	displacement wave transfer function parameter
k	radian wave number [m ⁻¹]

k_f	wave number of free wave [m^{-1}]
k_Σ	sum of radian wave numbers k_m and k_n [m^{-1}]
K	displacement wave transfer function parameter
l	distance from bottom to hinged point of wave generator [m]
L_0	deep water wavelength [m]
N	number of frequency components in Fourier series
p	pressure [Pa]
P	displacement wave transfer function parameter
$P(f)$	“power” spectral or variance density estimate [(units) ² / Hz]
Q	displacement wave transfer function parameter
R	displacement wave transfer function parameter
$R(\tau)$	autocorrelation function
S	spectral variance density [m^2 / Hz]
t	time [s]
T	wave record length [s]
$T^{(1)}$	first-order transfer function according to Biesel
u	horizontal, orbital wave velocity [m/s]
U	bound wave transfer function parameter
U_{10}	wind speed at 10 metres above water surface [m/s]
w	vertical, orbital wave velocity [m/s]
W	Donelan wave age parameter
x	horizontal coordinate [m]

X	waveboard position [m]
X_0	waveboard position at still water surface [m]
z	vertical coordinate [m]
α	wave spectrum parameter
β'	bound wave transfer function parameter
δ	second-order transfer function parameter
ϕ	velocity potential [m/s]
ϕ_{TMA}	TMA spectral parameter
γ	displacement wave transfer function parameter or wave spectrum parameter
η	water surface elevation [m]
λ	evanescent mode transfer function parameter
μ	dynamic viscosity [kg/m•s] or wave spectrum parameter
ν	number of degrees of freedom
π	transcendental constant
ρ	fluid density [kg/m ³]
τ	time lag [s]
ω	radian frequency [s ⁻¹]
ω_{Σ}	sum of radian frequencies ω_m and ω_n
ξ	long wave surface elevation [m]
$\zeta(t)$	stationary random function of time
Ω	second-order transfer function parameter

Ω_3	evanescent mode transfer function parameter
ϵ	ordering parameter

Notation

a_t	subscript t denotes partial differentiation
a_x	subscript x denotes partial differentiation
a_z	subscript z denotes partial differentiation
$a^{(n)}$	an n^{th} -order quantity
$ a $	modulus or amplitude
\mathbf{a}	a vector
m	subscript denoting the m^{th} wave component
n	subscript denoting the n^{th} wave component
$\Re\{\}$	real part
$\Im\{\}$	imaginary part
∇	grad operator
$f(a)$	function of a

Acknowledgments

I am indebted to many people who have provided various types of support over the past three years; the names of a few follow.

I would like to thank Dr. Jay Doering for both the opportunity to pursue graduate research and for the encouragement and mentoring that enabled me to complete this work. Being one of Jay's graduate students has truly been one of the highlights of my academic career.

My wife Glenda has been a great support and encouragement during this time. Her confidence in me and my abilities enabled me to persevere until the project was completed.

Many thanks go to my examining committee consisting of Dr. C. Booy from Civil and Geological Engineering and Dr. R. Azad from Mechanical and Industrial Engineering for their insightful questions and their contributions to this thesis.

My family has been a constant source of encouragement and understanding through my undergraduate years and on through the decision to enter graduate studies and continues today. Thank you.

Technician Roy Hartle of the Hydraulics Research and Testing Facility (HRTF) has been instrumental in running the laboratory component of this research. His technical expertise and dedication to seeing the job through to completion helped immensely.

Thanks to the Natural Sciences and Engineering Research Council (NSERC) for providing the funding that enabled me to pursue this research.

Finally, to everyone who asked if I was done yet when I was not for keeping me going. I can now finally say to all of them, "Yes, I am finished."

Chapter 1: Introduction

1.1 Background.

The laboratory wave flume, a long, relatively narrow channel with a wavemaker at one end and a wave energy absorption system at the other, is a common facility for the experimental study of water waves and their interaction with fixed and floating coastal structures, including the shoreline itself. Although the generated wavefield is often two-dimensional, this limitation is unimportant in many practical applications (e.g., cross-shore sediment transport, shore protection testing), and the use of a single planar wavemaker to produce waves is adequate. The 2-D characteristics of a wave flume must, however, be kept in mind when interpreting the results of model tests since not all the natural processes have been accounted for (*i.e.*, alongshore current). Three-dimensional wave fields can be created in a wave basin using a long segmented waveboard. In order to accurately simulate coastal phenomena, a “realistic” sea state is required.

The movement of the waveboard and the boundary condition at the waveboard give rise to numerous spurious second-order effects that can seriously corrupt or interfere with natural phenomena. In a natural wavetrain the non-linearity of the free-surface boundary conditions introduces sub- and superharmonics which are phase locked to the primary wave components. The subharmonics (or bound long waves) can generate the long period harbour oscillations, slow-drift motions of moored vessels and tension leg platforms, and sandbar formation due to sediment transport. The superharmonics introduce sharper-peaked crests and flatter troughs that are important for sediment transport due to wave

asymmetry and can be of importance for forces on offshore platforms. An incorrect (first-order) reproduction in the laboratory generates free waves at the same frequencies as the bound long and short waves, but travelling at free wave speed rather than at the wave group velocity. This difference in speed between the free and bound wave components results in spatial variations in the water surface fluctuations. A proper understanding of the complex nature of the sea state and its mechanical reproduction in the laboratory wave basin or flume have been the subject of intensive research over the past twenty years.

1.2. Literature Review.

Several investigators have studied the non-linear wavefield produced by finite-amplitude wavemakers using an approach based on the Stokes expansion procedure. The technique involves expressing the generated waveforms, associated velocity potentials, and, most recently, piston position as perturbation series, where the expansion parameter is related to wave steepness (Stokes, 1847). The use of a Stokes expansion results in a series of linear problems, one at each order of the perturbation approximating the non-linear problem. Most of the work on this problem has focused on including the second-order terms in the analysis.

Stokes' (1847) work included only the waveforms and the associated velocity potentials in the perturbation technique for regular waves. Only the second-order sum frequencies appear (difference frequencies vanish) and expressions for the second-order amplitude and phase were given. Biésel (1951) developed the first-order transfer function relating piston-type waveboard displacement and the resulting wave amplitude. He also

recognized and quantified the first-order local disturbances due to the horizontal velocity profile mismatch that results in the production of a second-order evanescent mode wave. In nature, the horizontal velocity profile is parabolic with zero velocity at the bottom boundary. In a laboratory, the planar wavemaker creates a uniform velocity profile.

Fontanet (1961) presented the first complete approach to second-order wavemaker theory for the waves forced by an oscillating plane wavemaker. Using a Lagrangian description he found the spurious superharmonics generated by a purely sinusoidal oscillation of the waveboard and described how to suppress these by adding a second-order superharmonic component to the first-order wavemaker control signal. His choice of a Lagrangian coordinate system makes the solution complicated to apply.

Longuet-Higgins and Stewart (1962,1964) were the first to point out that the variation of the radiation stress, which is defined as the excess flux of momentum due to the presence of waves, in grouped waves is the reason that long period waves are associated with wave groups. Their theory for the group-induced generation of long waves is based on the narrow-banded assumption. Ottesen Hansen (1978) and Ottesen Hansen *et al.* (1980) derived similar results to Longuet-Higgins and Stewart (1964) without the narrow banded restriction. The solution presented by Ottesen Hansen *et al.* (1980) uses a transfer function that gives the second-order contribution in terms of the interacting first-order wave components.

Madsen (1971) developed an approximate theory using a Stokes-like expansion for the suppression of spurious superharmonics in regular waves generated in fairly shallow water. His method suppressed spurious free waves by adding a second-order control signal to the first-order control signal. His solution is limited to relatively long waves.

Buhr Hansen *et al.* (1975) chose an empirical approach to pursue the second-order control signal for regular waves. He was able to determine both the amplitude and phase of a regular free second-order harmonic wave. For an irregular wavetrain expressed by a Fourier series, the large number of cross products of second-order makes it impossible to apply such an empirical approach.

Dean and Sharma (1981) developed a generalization including both subharmonics and superharmonics for directional waves. Their work included a second-order transfer function linking the second-order waves to the primary wave components.

Flick and Guza (1980) used a Stokes expansion to analyze the motion of a wavemaker that is hinged either on or below the channel bottom. They evaluated the relationship between the second-harmonic free waves forced by the wavemaker and the second-harmonic Stokes waves using regular waves and wave groups.

Hudspeth and Sulisz (1991) derived the complete second-order solution to the wavemaker problem using an eigenfunction expansion approach. The solution considered monochromatic wave paddle motion with special emphasis on Stokes drift and return flow

in wave flumes. Their formulation included new terms previously neglected in the Stokes type analyses. Sulisz and Hudspeth (1993) presented an eigenfunction expansion complete to second-order for the two-dimensional wave motion forced by a sinusoid wavemaker motion. They experimentally verified the work of Hudspeth and Sulisz (1991) in a 2-D wave basin and calculated second-order amplitudes for the free wave and the Stokes wave. Mobayed and Williams (1994) extended the theory of Hudspeth and Sulisz (1991) to cover bichromatic paddle motion. Their derivation explicitly included the difference frequency second-order effects unlike Hudspeth and Sulisz (1991) and Sulisz and Hudspeth (1993). Their results were confirmed numerically.

For random waves, Sand (1982) calculated the second-order subharmonic control signal for a piston type wavemaker needed to suppress three spurious long wave components created using first-order wave generation techniques without requiring the narrow band assumption. Barthel *et al.* (1983) gave a more detailed description of the theory of Sand (1982) and extended it to include a rotating waveboard motion, restricting the center of rotation to a point at or below the bottom of the flume. Sand and Donslund (1985) gave the theoretical extension to Barthel *et al.* (1983), needed to include the case of a rotating waveboard with the hinge located above the flume bottom.

Extending the basic principles outlined in Flick and Guza (1980), Sand and Mansard (1986a, 1986b) developed the theoretical transfer functions, similar to those used by Sand (1982), necessary to reproduce correctly the higher harmonics in an irregular sea state. A second-order control signal was calculated in order to ensure the correct reproduction of

the wave profile without any spurious, higher-harmonic free wave effects. Their technique is valid for translatable as well as rotating waveboards.

In order to make the wave generation algorithm more efficient, Klopman and Van Leeuwen (1990) used a technique based on the perturbation method of multiple scales to derive the formulas for the second-order wavemaker control signal. The method of multiple scales pursues the corrections in the time domain unlike the frequency domain methods of Sand (1982), Barthel *et al.* (1993), Sand and Donslund (1985), and Sand and Mansard (1986a, b). The amount of work to generate the second-order corrections with their method is proportional to the amount of work to generate the first-order signal. In previously used second-order frequency domain methods, this amount of work was proportional to the square of the effort for generating the first-order signal. Their method is of limited utility since it assumes a narrow spectral bandwidth for the first-order waves.

For a substantial simplification of the theory, the evanescent modes can be ignored when the waveboard motion makes a good fit to the velocity profile of the desired progressive waves. Situations where this approximation fails are often encountered. Schäffer (1994) quantified the error introduced by ignoring the effects of evanescent modes in second-order wave generation. Schäffer (1996) recently presented the complete second-order wavemaker theory for irregular waves. A complex representation was chosen to facilitate and simplify the theoretical calculations. A method known as the asymptotic summation method (Schäffer, 1993) was included to quickly find the sum of the infinite series that appear in his second-order solution. The theory was verified for a piston-type wavemaker

using regular waves, wave groups, and irregular waves. This research appeared too late (*i.e.*, January, 1996) to be included in the present work.

1.3. Objectives of this Research.

The objectives of this research are:

- i) to present a theoretical framework for the generation of a 2-D laboratory wavefield correct to second-order using the long wave correction algorithms of Sand (1982), Barthel *et al.* (1983), Sand and Donslund (1985), and the short wave correction algorithms of Sand and Mansard (1986a, b),
- ii) to create a user-interactive software package in MATLAB, based on the algorithms presented in (i) to generate waves correct to second-order in the laboratory,
- iii) to test and calibrate the software package developed in (ii),
- iv) to study the effects of using a thresholding technique to improve algorithm efficiency
- v) to use bispectral techniques to test the algorithms.

In the following chapter a theoretical basis for including second-order effects in the mechanical generation of a wave field free of spurious effects is presented. An overview of the MATLAB-based software package including an explanation of the thresholding technique found is found in chapter 3. The experimental setup and the wave data generated and recorded are described in chapter 4. Chapter 5 includes a brief theoretical discussion of the bispectrum and its application to the study of triad interactions. The bispectral analysis of the recorded wave data are also included. A summary of the results, conclusions and recommendations for future work are given in chapter 6.

Chapter 2: Wavemaker Theory

2.1. Governing Equations.

The Navier-Stokes equation

$$\mathbf{u}_t + \mathbf{u} \cdot \nabla \mathbf{u} = -\frac{1}{\rho} \nabla p + \frac{\mu}{\rho} \nabla^2 \mathbf{u} + \mathbf{g} \quad (2.1)$$

is the foundation of fluid mechanics. In the usual notation, ρ is the fluid density, p is the pressure, μ is the dynamic viscosity, $\mathbf{u} = (u, v, w)$ the x , y , and z components of velocity, respectively, and \mathbf{g} is the acceleration due to gravity. The x - y axes lie in a horizontal plane and the z -axis points vertically upward. The motion of a Newtonian fluid is well described by the Navier-Stokes equation, however, problems arise in trying to solve this equation. For the case of surface gravity waves, finding a solution to this equation is further complicated by the unknown position of the free surface and the relatively complicated boundary conditions to be applied there.

To make the problem tractable, the following simplifying assumptions are applied:

- i) the flow is irrotational,
- ii) the flow is incompressible,
- iii) the fluid is inviscid,
- iv) surface tension is negligible,
- v) ρ and g are temporally and spatially constant,
- vi) the waves propagate in the positive x -axis direction, and
- vii) the bottom is flat and impermeable.

The resulting equations describing waves propagating in a flat bottom flume and equipped with a rotating and/or translating waveboard are given in terms of the velocity potential $\phi(x,z,t)$, defined by (Barthel *et al.*, 1983)

$$u = \frac{\partial \phi}{\partial x}, v = \frac{\partial \phi}{\partial z} \quad (2.2a)$$

$$\Delta \phi = 0 \quad \text{everywhere in the fluid} \quad (2.2b)$$

$$\phi_t + \frac{1}{2}(\phi_x^2 + \phi_z^2) + g\eta = 0 \quad \text{for } z = \eta \quad (2.2c)$$

$$\eta_t + \phi_x \eta_x - \phi_z = 0 \quad \text{for } z = \eta \quad (2.2d)$$

$$\phi_z = 0 \quad \text{for } z = -h \quad (2.2e)$$

$$\text{condition at the waveboard} \quad \text{for } x = X(z,t) \quad (2.2f)$$

where $\phi = \phi(x,z,t)$ velocity potential

$\eta = \eta(x,t)$ water surface elevation

g = acceleration of gravity

h = mean water depth

x, z = horizontal and vertical coordinates

t = time

The position of the waveboard, X , is given as

$$X(z,t) = f(z)X_0(t) \quad (2.3)$$

$$\text{with } f(z) = 1 + \frac{z}{h+l} \quad (2.4)$$

where h is the water depth and l is the distance to a fictitious waveboard pivot point. The definition sketch shown in Figure 2.1 covers the types of wavemakers considered by the governing equations above. It appears that there are two limiting cases: a flap, hinged at

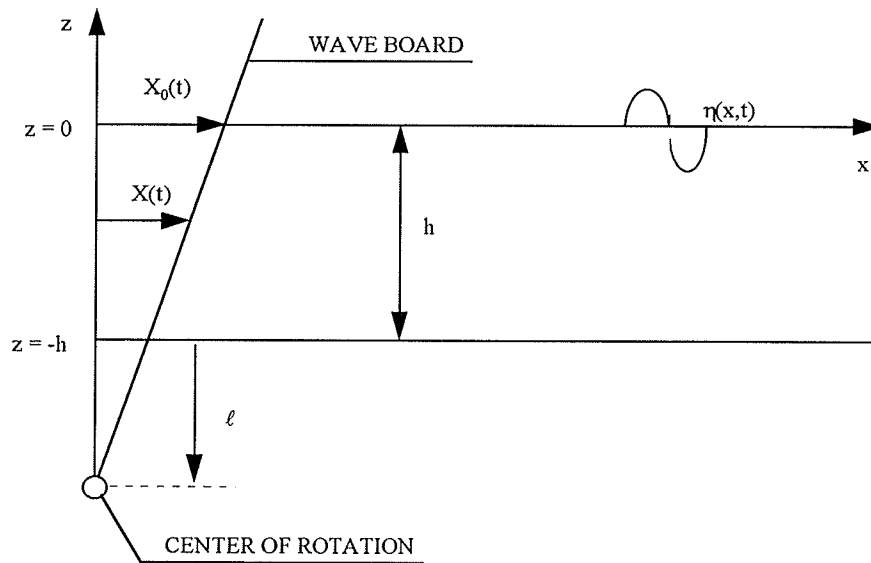


Figure 2.1 Definition sketch for wave generators with translatory, rotational, or combined modes of operation.

the bottom of the wave flume ($l = 0$) and a piston-type wavemaker ($l = \infty$). Values for l in between these conditions relate to a combined rotating and translating motion of the waveboard. Elevated piston and flap wavemakers require additional terms in the governing equations.

Taylor series expansions are applied to the basic equations and the boundary conditions to obtain boundary conditions at the waveboard, where $x = 0$ and $z = 0$. X_0 , ϕ , and η are expanded in terms of an ordering parameter, ϵ , which results in first- and second-order phenomena

$$\eta = \epsilon \eta^{(1)} + \epsilon^2 \eta^{(2)} \quad (2.5a)$$

$$\phi = \epsilon \phi^{(1)} + \epsilon^2 \phi^{(2)} \quad (2.5b)$$

$$X_0 = \epsilon X_0^{(1)} + \epsilon^2 X_0^{(2)}. \quad (2.5c)$$

This method of solution results in the following first- and second-order equations

First-order equations:

$$\Delta \phi^{(1)} = 0 \quad (2.6a)$$

$$\phi_u^{(1)} + g \phi_z^{(1)} = 0 \quad \text{for } z = 0 \quad (2.6b)$$

$$\phi_z^{(1)} = 0 \quad \text{for } z = -h \quad (2.6c)$$

$$\phi^{(1)} = f(z) \frac{dX_0^{(1)}}{dt} \quad \text{for } x = 0 \quad (2.6d)$$

Second-order equations

$$\Delta\phi^{(2)} = 0 \quad (2.7a)$$

$$\phi_n^{(2)} + g\phi_z^{(2)} = -\eta^{(1)} \left\{ g\phi_{zz}^{(1)} + \phi_{tz}^{(1)} \right\} - \eta_t^{(1)} \phi_{tz}^{(1)} + \phi_x^{(1)} \left\{ g\eta_x^{(1)} + \phi_{xt}^{(1)} \right\} + \phi_z^{(1)} \phi_{zt}^{(1)} \quad \text{for } z = 0 \quad (2.7b)$$

$$\phi_z^{(2)} = 0 \quad \text{for } z = -h \quad (2.7c)$$

$$\phi^{(2)} = f(z) \frac{dX_0^{(2)}}{dt} - X_0^{(1)} \left\{ f(z)\phi_{xx}^{(1)} - \frac{1}{h+l}\phi_z^{(1)} \right\} \quad \text{for } x = 0 \quad (2.7d)$$

Equations (2.6a) - (2.7d) can be solved for the case where the first-order wave motion, $\in\eta^{(1)}$, which is far from the wavemaker, is given by

$$\in\eta^{(1)}(x,t) = \sum_{n=1}^N \left\{ a_n \cos(\omega_n t - k_n x) + b_n \sin(\omega_n t - k_n x) \right\} \quad (2.8)$$

where N is the total number of wave components. The first-order equations are solved for $\phi^{(1)}$ and $X_0^{(1)}$. Substituting the first-order solutions into the second-order equations, result in sinusoidal terms with sum and difference frequencies. The second-order equations are then solved with the additional condition that no free waves may exist to second-order, *i.e.*, find $X_0^{(2)}$.

2.2. First-Order Solution.

Since the first-order equations are linear in $\phi^{(1)}$, the terms in (2.8) can be treated individually, and then summed to give $\phi^{(1)}$ and $X_0^{(1)}$. Using this approach, we look for a solution of the form

$$X_0^{(1)} = \sin \omega t. \quad (2.9)$$

The corresponding potential $\phi^{(1)}$ (solution of the first-order equations) is (Flick and Guza, 1980)

$$\phi^{(1)} = B \frac{\cosh k(z+h)}{\cosh kh} \sin(kx - \omega t) + \sum_{j=1}^{\infty} C_j \frac{\cos l_j(z+h)}{\cos l_j h} e^{-l_j x} \cos \omega t \quad (2.10a)$$

where

$$k \text{ is the positive and real root of } \omega^2 = gk \tanh kh \quad (2.10b)$$

$$B = \frac{\omega}{k} \cosh kh \frac{\int_{-h}^0 f(z) \cosh k(z+h) dz}{\int_{-h}^0 \cosh^2 k(z+h) dz} \quad (2.10c)$$

$$l_j \text{ is the positive and real root of } -\omega^2 = gl_j \tan l_j h \quad (2.10d)$$

$$\text{with } (j - \frac{1}{2})\pi < l_j h < j\pi, \quad j = 1, 2, 3, \dots \quad (2.10e)$$

$$C_j = -\frac{\omega}{l_j} \cos(l_j h) \frac{\int_{-h}^0 f(z) \cos l_j(z+h) dz}{\int_{-h}^0 \cos^2 l_j(z+h) dz} \quad (2.10f)$$

For the waveboard motion, the general solution of the first-order equations is given by

$$\in X_0^{(1)} = \sum_{n=1}^N \frac{g}{B_n \omega_n} \{a_n \sin \omega_n t - b_n \cos \omega_n t\}. \quad (2.11)$$

2.3. Second-Order Solution : Long Waves.

Due to the linearity of the second-order equations (2.7a)-(2.7d) in $\phi^{(2)}$, it is possible to write $\phi^{(2)}$ as a superposition of three potentials (Barthel *et al.*, 1983):

$$\phi^{(2)} = \phi^{(21)} + \phi^{(22)} + \phi^{(23)}. \quad (2.12)$$

The potential functions composing $\phi^{(2)}$ have to satisfy the equations below, which make $\phi^{(2)}$ satisfy the original second-order equations.

$\phi^{(21)}$ has to satisfy the following equations (Barthel *et al.*, 1983):

$$\Delta\phi^{(21)} = 0 \quad (2.13a)$$

$$\phi_{tt}^{(21)} + g\phi_z^{(21)} = -\eta^{(1)}\{g\phi_{zz}^{(1)} + \phi_{ttz}^{(1)}\} - \eta_t^{(1)}\phi_{tz}^{(1)} + \phi_x^{(1)}\{g\eta_{tx}^{(1)} + \phi_{xt}^{(1)}\} + \phi_z^{(1)}\phi_{zt}^{(1)} \text{ for } z = 0 \quad (2.13b)$$

$$\phi_z^{(21)} = 0 \quad \text{for } z = -h \quad (2.13c)$$

$$\text{no condition at the wave board} \quad \text{for } x = 0 \quad (2.13d)$$

Physically, this means that $\phi^{(21)}$ corresponds to the second-order long waves that are bound to the wave groups, see Ottesen Hansen (1978). The absence of a boundary condition at the waveboard indicates that the solution is representative of progressive waves in general, including those found in nature.

$\phi^{(22)}$ has to satisfy the following equations (Barthel *et al.*, 1983):

$$\Delta\phi^{(22)} = 0 \quad (2.14a)$$

$$\phi_{tt}^{(22)} + g\phi_z^{(22)} = 0 \quad \text{for } z = 0 \quad (2.14b)$$

$$\phi_z^{(22)} = 0 \quad \text{for } z = -h \quad (2.14c)$$

$$\phi_x^{(22)} = -X_0^{(1)}\left\{f(z)\phi_{xx}^{(1)} - \frac{1}{h+l}\phi_z^{(1)}\right\} - \phi_x^{(21)} \quad \text{for } x = 0 \quad (2.14d)$$

The waveboard boundary condition (2.14d) indicates that there are several types of free second-order waves arising from the terms on the right-hand side. The first term,

$$-X_0^{(1)}\left\{f(z)\phi_{xx}^{(1)} - \frac{1}{h+l}\phi_z^{(1)}\right\},$$

appears as the waveboard moves out of its mean position (*i.e.*, $X_0^{(1)} \neq 0$). Two free long waves are represented: one is associated with first-order local disturbances and the other is due to waveboard displacement. The second term, $-\phi_x^{(21)}$, originates as a reflection on the

waveboard of the group bounded long waves which are naturally generated. The backward orbital velocities found under the long wave troughs reflect off the waveboard with the same magnitude but opposite phase as the bound waves. This third type of free long waves are known as “parasitic long waves”. All three disturbances are spurious long waves, which have to be suppressed by means of a second-order waveboard displacement $X_0^{(2)}$.

$\phi^{(23)}$ has to satisfy the following equations (Barthel *et al.*, 1983):

$$\Delta\phi^{(23)} = 0 \quad (2.15a)$$

$$\phi_{tt}^{(23)} + g\phi_z^{(23)} = 0 \quad \text{for } z = 0 \quad (2.15b)$$

$$\phi_z^{(23)} = 0 \quad \text{for } z = -h \quad (2.15c)$$

$$\phi_x^{(23)} = f(z) \frac{dX_0^{(2)}}{dt} \quad \text{for } x = 0 \quad (2.15d)$$

These equations determine the second-order waveboard motions, $X_0^{(2)}$, which are necessary for the correct generation of grouped waves with only the bound long waves present. Equations (2.15a) - (2.15d) provide the compensation for the free waves described by $\phi^{(22)}$ (Equations (2.14a) - (2.14d)).

In order to solve these second-order equations, the first-order solutions $\eta^{(1)}$, $\phi^{(1)}$ and $X_0^{(1)}$ have to be substituted into the right-hand side of the respective equations. However, because they are linear with respect to $\phi^{(2)}$, it is sufficient to consider only two first-order components. Afterwards, superposition can be applied to include the contributions of all possible combinations of frequencies in a realistic wavetrain.

The final solution is seen to be the result of the superposition of all the combinations of the two first-order components. The complete second-order paddle motion is then given by

$$\epsilon^2 X_0^{(2)} = \sum_{n=1}^{N-1} \sum_{m=n+1}^N \epsilon^2 X_{0, nm}^{(2)} \quad (2.16)$$

It should be noted that the total waveboard displacement (including the second-order long wave correction) is given by

$$X(t) = f(z) \left(\epsilon X_0^{(1)} + \epsilon^2 X_0^{(2)} \right). \quad (2.17)$$

Calculation of the second-order long waves and the second-order piston position are based on a Fourier decomposition of the primary wavetrain. The long wave elevations are found from the sum

$$\xi(t) = \sum_{n=m^*}^{\infty} \sum_{m=n^*}^{\infty} \xi_{nm}(t), \text{ with } m^* = \frac{f^*}{f_0} \quad (2.18)$$

where $f_0 = 1/T$ is the frequency interval in the Fourier decomposition, T is the length of the record, and f^* is the lowest frequency in the short wave spectrum. Thus, $\xi(t)$ is the sum of contributions from all pairs of frequencies in the decomposition.

It is sufficient to consider a single long wave contribution generated by one frequency pair, f_n and f_m , with the elevations $\eta_n(t)$ and $\eta_m(t)$, respectively. Such a pair of waves forms a wave group

$$\begin{aligned} \eta_{nm}(t) = \eta_n + \eta_m = & a_n \cos(\omega_n t - k_n x) + b_n \sin(\omega_n t - k_n x) \\ & + a_m \cos(\omega_m t - k_m x) + b_m \sin(\omega_m t - k_m x) \end{aligned} \quad (2.19)$$

in which a is the wave amplitude and ω is the radial frequency. The second-order long wave generated by this group becomes

$$\xi_{nm}(t) = G_{nm}^- h \left[\left(\frac{a_n a_m + b_n b_m}{h^2} \right) \cos(\Delta\omega_{nm} t - \Delta k_{nm} x) + \left(\frac{a_m b_n - a_n b_m}{h^2} \right) \sin(\Delta\omega_{nm} t - \Delta k_{nm} x) \right] \quad (2.20)$$

where G_{nm}^- is a transfer function, $\Delta\omega_{nm} = \omega_n - \omega_m$, and $\Delta k_{nm} = k_n - k_m$ are long wave quantities. The long wave frequency is $\Delta f_{nm} = f_n - f_m = \Delta\omega_{nm}/2\pi$.

The dimensionless transfer function $G_{nm}^- h$ is given for a piston type wave generator as (Ottesen Hansen, 1978; Sand, 1982):

$$G_{nm}^- h = \frac{\left[\frac{4\pi^2 D_n D_m \Delta k_{nm} h \cosh(\Delta k_{nm} h)}{\cosh(k_n h + k_m h)} + \frac{\Delta k_{nm} h (D_n - D_m) (k_n h D_m + k_m h D_n) \coth(\Delta k_{nm} h)}{2 D_n D_m} - 2\pi^2 (D_n - D_m)^2 \Delta k_{nm} h \right]}{4\pi^2 (D_n - D_m)^2 \coth(\Delta k_{nm} h) - \Delta k_{nm} h} \quad (2.21)$$

where $D_n = (h/g)^{1/2} f_n$ and $D_m = (h/g)^{1/2} f_m$, with g being the gravitational acceleration constant. The dimensionless transfer function $G_{nm}^- h$ is plotted as a function of h / L_0 for several values of $\Delta f / f_m$ in Figure 2.2.

The correct second-order piston positions for the reproduction of group-induced long waves in a natural wavetrain are

$$X^{(2)}(t) = \sum_{n=m+1}^{\infty} \sum_{m=m^*}^{\infty} X_{nm}^{(2)}(t) \quad (2.22)$$

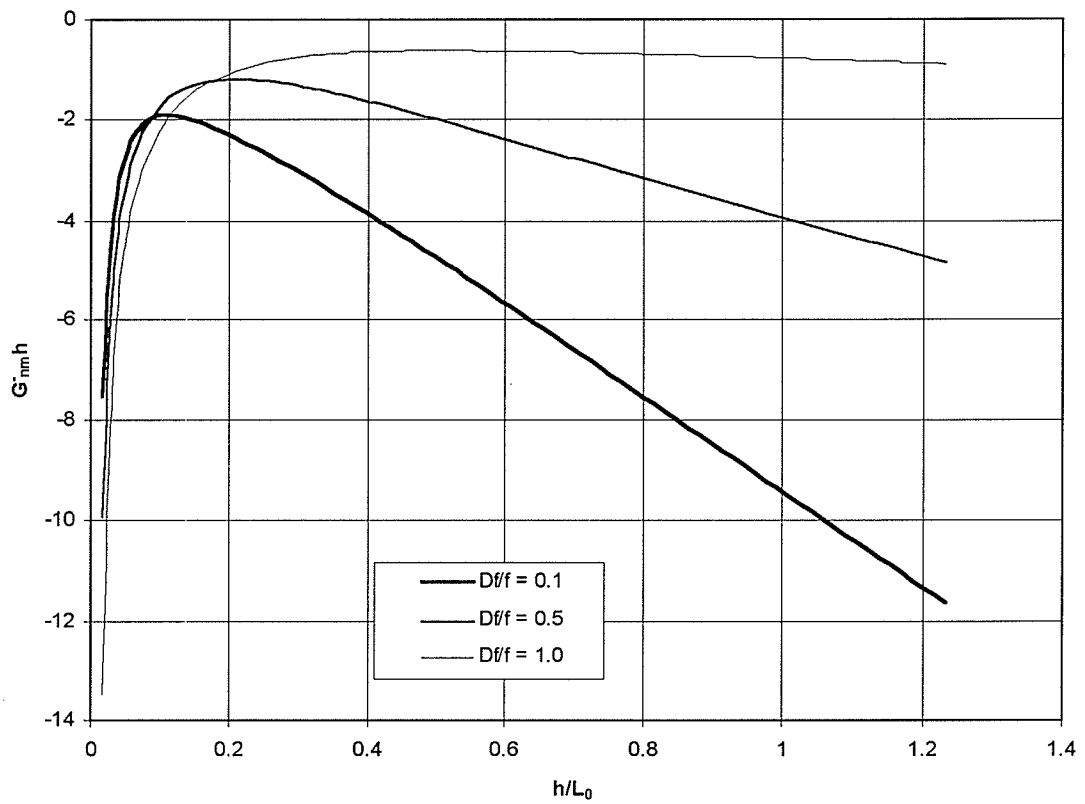


Figure 2.2 Long wave transfer function $G^-_{nm} h$ for a pair of wave components f_n and f_m as a function of h/L_0 .

The solution to the second-order equations can be written as (Sand, 1982):

$$\begin{aligned} \frac{X_{nm}^{(2)}(t)}{h} = & \left[\left(\frac{a_n b_m - a_m b_n}{h^2} \right) F_1 h + \left(\frac{a_n a_m + b_n b_m}{h^2} \right) F_{23} h \right] \cos \Delta \omega_{nm} t \\ & + \left[\left(\frac{a_n a_m + b_n b_m}{h^2} \right) F_1 h + \left(\frac{a_n b_n - a_n b_m}{h^2} \right) F_{23} h \right] \sin \Delta \omega_{nm} t \end{aligned} \quad (2.23)$$

For the second-order correction calculations, the dimensionless function $F_1 h$ is

$$F_1 h = F_{11} h + F_{12} h \quad (2.24)$$

where

$$F_{11} h = \frac{G_{nm} h \Delta k_f h \left[(\Delta k_{nm} h - \Delta k_f h) \sinh(\Delta k_{nm} h + \Delta k_f h) + (\Delta k_{nm} h + \Delta k_f h) \sinh(\Delta k_{nm} h - \Delta k_f h) \right]}{2(\Delta k_{nm}^2 h^2 - \Delta k_f^2 h^2) \sinh(\Delta k_{nm} h) \sinh(\Delta k_f h)} \quad (2.25)$$

and

$$\begin{aligned} F_{12} h = & \frac{f_m \Delta k_f h k_m h (1 + G_n) \left[\delta k_m^- h \sinh(\delta k_m^+ h) + \delta k_m^+ h \sinh(\delta k_m^- h) \right]}{\Delta f 8 (k_m^2 h^2 - \Delta k_f^2 h^2) \sinh(\Delta k_f h) \sinh(k_m h) \tanh(k_n h)} \\ & + \frac{f_n \Delta k_f h k_n h (1 + G_m) \left[\delta k_n^- h \sinh(\delta k_n^+ h) + \delta k_n^+ h \sinh(\delta k_n^- h) \right]}{\Delta f 8 (k_n^2 h^2 - \Delta k_f^2 h^2) \sinh(\Delta k_f h) \sinh(k_n h) \tanh(k_m h)} \end{aligned} \quad (2.26)$$

The free long wave number Δk_f is derived from $(\Delta \omega_{nm})^2 = g \Delta k_f \tanh(\Delta k_f h)$ and $\delta k_m^\pm = k_m \pm \Delta k_f$. The function $F_{11} h$ is the contribution to the second-order piston position that eliminates the free parasitic long wave resulting from a reflection off the waveboard of the natural rearward orbital velocities found underneath the bound group long wave trough. This reflected wave is exactly out of phase with the bound long wave at the waveboard but travels with a free wave velocity resulting in a location-dependent distortion of the long wave effects. The $F_{12} h$ function corrects for the free long wave appearing as a result of the waveboard moving out of its mean position, $x = 0$. It has thus been historically

referred to as the displacement function. The dimensionless functions $F_{11}h$ and $F_{12}h$ are plotted versus h/L_0 for several values of $\Delta f/f_m$ in Figure 2.3 and Figure 2.4, respectively. The sum of these two functions, F_1h , is shown in Figure 2.5. It is interesting to note that in shallow water the $F_{11}h$ function dominates, while in deep water the $F_{12}h$ function is the dominant one.

The function $F_{23}h$ used in the piston position equation above can be written in the form

$$F_{23}h = F_2h(F_{3,m} - F_{3,n}) \quad (2.27)$$

$$\text{in which } F_2h = \frac{\Delta k_f h (1 + G_n)(1 + G_m)}{8 \tanh(k_n h) \tanh(k_m h)}, \quad G_m = \frac{2k_m h}{\sinh(2k_m h)} \quad (2.28)$$

and

$$F_{3,m} = \frac{f_m}{\Delta f} \sum_{j=1}^{\infty} \frac{2k_j h \sin(k_j h) \left[k_j h \sin(k_j h) \coth(\Delta k_f h) + \Delta k_f h \cos(k_j h) \right]}{(k_j^2 h^2 + \Delta k_f^2 h^2) \left[\sin(k_j h) \cos(k_j h) + k_j h \right]} \quad (2.29a)$$

in which $k_j h$ is found as the solution to

$$\frac{4\pi^2 h f_m^2}{g} = -k_j h \tan(k_j h), \quad \text{with } \left(j - \frac{1}{2}\right)\pi < k_j h < j\pi \quad (2.29b)$$

The $F_{23}h$ function is the contribution that eliminates the free second-order progressive waves that originate from first-order local disturbances as described by Biésel (1951). These waves occur as a direct result of the horizontal velocity profile mismatch between natural waves and those generated by a planar wavemaker. Sand (1982) has shown that the magnitude of the F_{23} correction is sufficiently small when compared to the magnitude of F_1 to be considered insignificant for the purposes of laboratory testing.

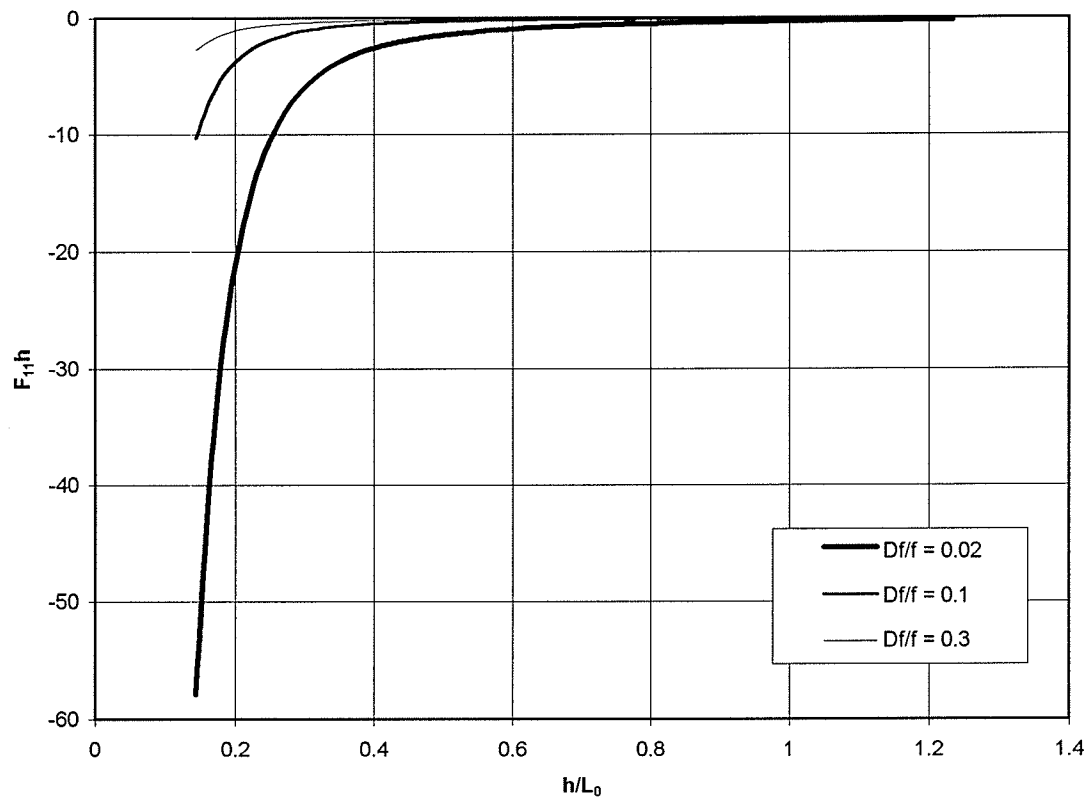


Figure 2.3 Long wave transfer function $F_{11}h$ for a pair of wave components f_n and f_m as a function of h/L_0 .

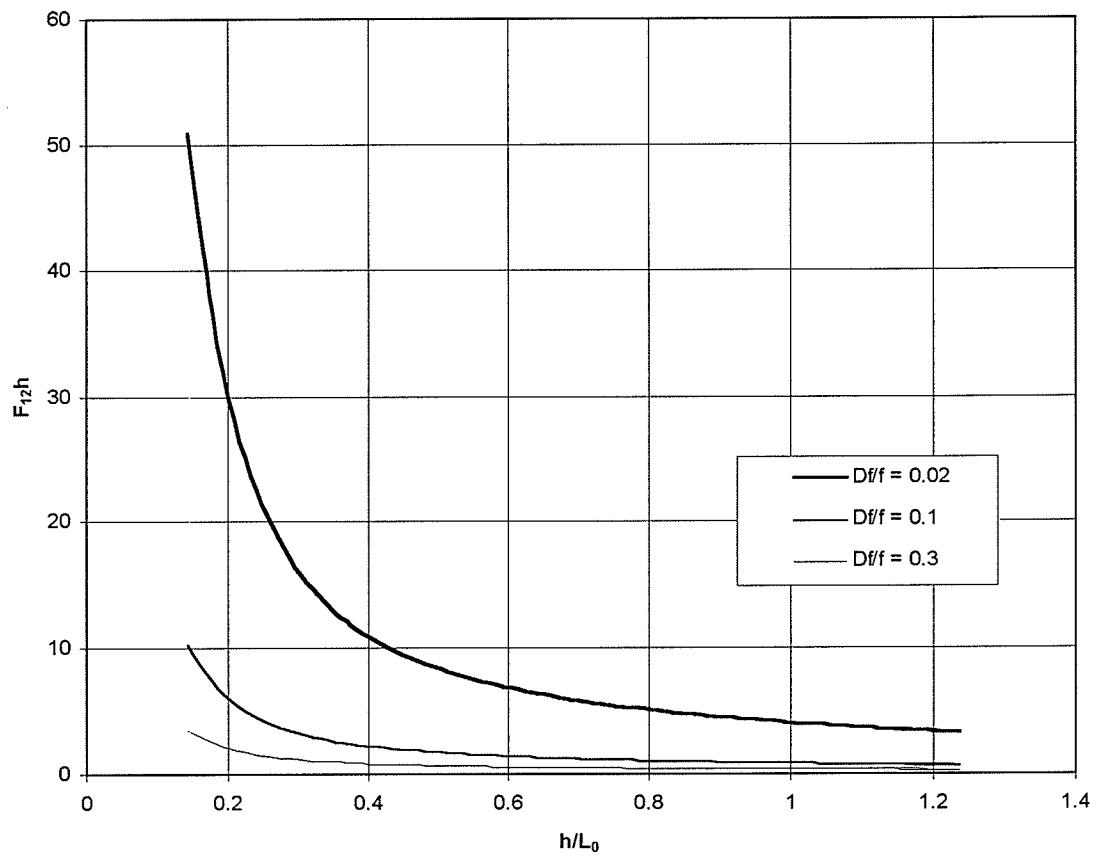


Figure 2.4 Long wave transfer function $F_{12}h$ for a pair of wave components f_n and f_m as a function of h/L_0 .

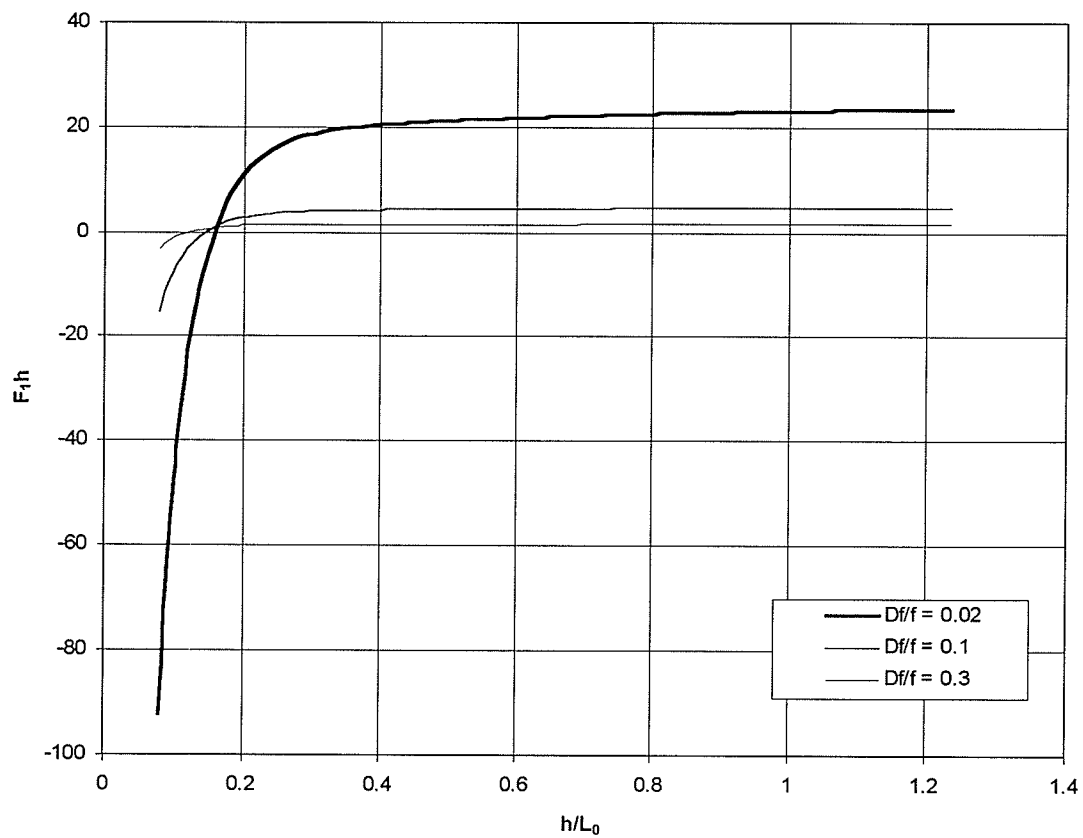


Figure 2.5 Long wave transfer function $F_j h$ for a pair of wave components f_n and f_m as a function of h/L_0 .

2.4. Second-Order Corrections : Short Waves.

The Laplace equation with a second-order surface condition is solved for a first-order wavetrain, $\eta^{(1)}$, described by a Fourier series. To simplify the calculations, the solution is found for pairs of frequencies and superposition is used to combine the results for all possible frequency sums. The following wave group is considered

$$\begin{aligned} \eta_{nm}^{(1)}(t) = & a_n \cos(\omega_n t - k_n x) + b_n \sin(\omega_n t - k_n x) \\ & + a_m \cos(\omega_m t - k_m x) + b_m \sin(\omega_m t - k_m x) \end{aligned} \quad (2.30)$$

in which a is the wave amplitude, ω is the radial frequency, k is the radial wave number ($=2\pi/L$, with wavelength L), x is the horizontal coordinate and m, n are the frequency subscripts of the two components selected from the Fourier series. Taking the wave group in Equation (2.18) as a kernel of the Fourier series the solution for the second-order control signal has the form:

$$\begin{aligned} X_{nm}^{(2)}(t) = & \left((a_n b_m + a_m b_n) F_1 + (a_n a_m - b_n b_m) F_{23} \right) \cos(\omega_\Sigma t) - \\ & \left((a_n a_m - b_n b_m) F_1 - (a_n b_m + a_m b_n) F_{23} \right) \sin(\omega_\Sigma t) \end{aligned} \quad (2.31a)$$

in which

$$F_1 = F_{11} + F_{12} \quad \text{and} \quad F_{23} = F_2 (F_{3,m} + F_{3,n}) \quad (2.31b)$$

and

$$\omega_\Sigma = \omega_n + \omega_m \quad (2.31c)$$

The function F_I , which converts the first-order Fourier amplitudes into a second-order correction consists of two parts, F_{I1} and F_{I2} . The first part, F_{I1} , is needed as a direct result of the bounded harmonics in the wavetrain. It allows $\eta_{HB}^{(2)}(t)$ to exist without spurious effects, which would otherwise appear as the reflection on the waveboard of the second-order bound components. With no flow through the waveboard, the natural

rearward orbital velocities underneath a wave trough are reflected off the waveboard and travel with a free wave velocity, resulting in a location-dependent distortion of the bound short wave effects, which travel with the wave group velocity. The dimensionless expression for F_{11} is (Sand and Mansard, 1986a):

$$F_{11}h = \left[G_{nm}^+ h U k_f^2 h^2 (k_f h \tanh k_f h - k_\Sigma h \tanh k_\Sigma h) (1 + l/h) \right] / \left[(k_\Sigma^2 h^2 - k_f^2 h^2) \tanh k_\Sigma h (k_f h (1 + l/h) \tanh k_f h - 1 + \beta^l / \cosh k_f h) \right] \quad (2.32a)$$

where $k_\Sigma = k_n + k_m$ (2.32b)

k_f is the free wave number from $(\omega_\Sigma)^2 = g k_f \tanh k_f h$, (2.32c)

$$\beta^l = \begin{cases} 1 & \text{for } l \geq 0 \\ \cosh k_f l & \text{for } l \leq 0 \end{cases} \quad (2.32d)$$

$$U = \frac{k_\Sigma h \tanh k_\Sigma h}{k_f h \tanh k_f h} \left(1 + \frac{k_n h k_m h (1 + \tanh k_n h \tanh k_m h)}{4 G_{nm}^+ h \sqrt{k_n h k_m h \tanh k_n h \tanh k_m h}} - \frac{k_f h \tanh k_f h}{4 G_{nm}^+ h} \right) \quad (2.32e)$$

G_{nm}^+ is a second-order transfer function for the primary frequencies $f_n + f_m$ expressed in dimensionless form as (Sand and Mansard, 1986a):

$$G_{nm}^+ h = \left\{ \left[2(\alpha_n + \alpha_m)^2 (k_n h k_m h / \alpha_n \alpha_m - 4\pi^2 \alpha_n \alpha_m) + (\alpha_n + \alpha_m) (k_m^2 h^2 / \alpha_m + k_n^2 h^2 / \alpha_n - 4\pi^2 (\alpha_n^3 + \alpha_m^3)) \right] / \left[4\pi (\alpha_n + \alpha_m)^2 - \Omega \right] + \left[4\pi^2 \alpha_n^2 \alpha_m^2 (1 + \alpha_n / \alpha_m + \alpha_m / \alpha_n) - k_n h k_m h \right] / 4\pi \alpha_n \alpha_m \right\} \delta \quad (2.33)$$

in which $\Omega = 2k_\Sigma h \tanh k_\Sigma h$, $\alpha_m = (h / L_{0,m})^{1/2}$, $\alpha_n = (h / L_{0,n})^{1/2}$ and L_0 is the deep water wavelength. Noting that the self-self interaction binds only half the second-order

component of an interaction involving two frequencies slightly separated in the frequency domain, consequently, the transfer function, G_{nm}^+ , includes the multiplier δ , which has the value:

$$\delta = \begin{cases} 1 & \text{for } n \neq m \\ 1/2 & \text{for } n = m \end{cases} \quad (2.34)$$

The transfer function $G_{nm}^+ h$ is plotted in Figure 2.6 as a function of h / L_0 (for the m -component, $m < n$) and the ratio f_n / f_m . The curve for $f_n / f_m = 1.0$ corresponds to the self-interaction of one regular wave.

The second part, F_{12} , is related to the $X^{(1)}\phi_{xx}^{(1)}$ and $X^{(1)}\phi_z^{(1)}$ terms of the waveboard boundary condition (Equation (2.7d)). This so-called “displacement wave” is caused by the waveboard moving out of its mean position. The product of paddle displacements and both the horizontal, orbital accelerations in the waves and the vertical velocities, respectively, form a second-order higher harmonic contribution. To eliminate these free wave components of frequency ω_Σ , the control signal includes the function F_{12} . In dimensionless form this function is (Sand and Mansard, 1986a):

$$F_{12} h = K \left(I_m / T_n^{(1)} + (f_n / f_m) I_n / T_m^{(1)} \right) \quad (2.35a)$$

in which

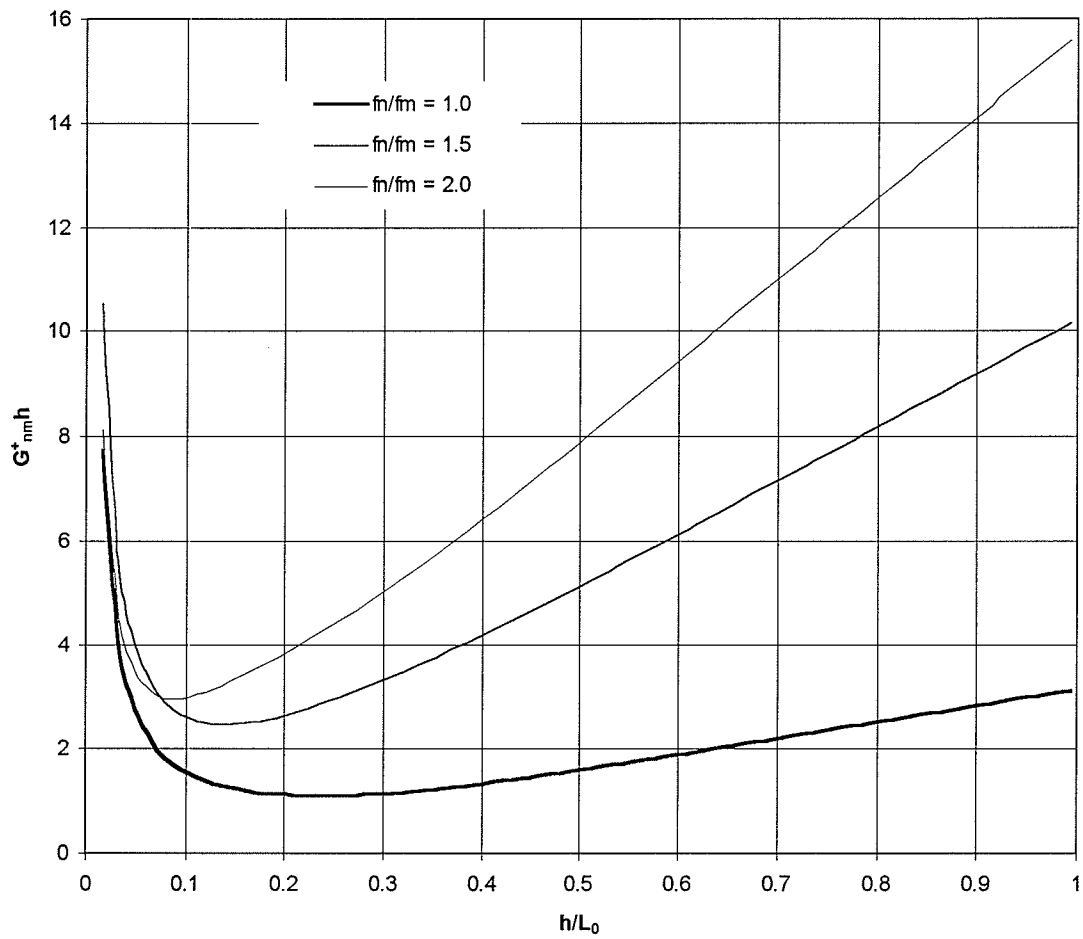


Figure 2.6 Short wave transfer function $G_{nm}^+ h$ for a pair of wave components f_n and f_m as a function of h/L_0 .

$$K = \frac{k_f^2 h^2 (1 + l/h)}{(k_f h (1 + l/h) \sinh k_f h - \cosh k_f h + \beta') (f_n / f_m + 1)} \quad (2.35b)$$

$$I_m = \frac{k_m h}{2 \sinh k_m h} (P_m + Q_m + R_m) \quad (2.35c)$$

$$P_m = \frac{\sinh(k_m + k_f)h + \delta_1}{2(k_m h + k_f h)} + \frac{\sinh(k_m - k_f)h + \delta_2}{2(k_m h - k_f h)} \quad (2.35d)$$

$$Q_m = \frac{\gamma_1 - \cosh(k_m + k_f)h}{2(k_m h + k_f h)^2 (1 + l/h)} + \frac{\gamma_2 - \cosh(k_m - k_f)h}{2(k_m h - k_f h)^2 (1 + l/h)} \quad (2.35e)$$

$$R_m = \frac{k_m h (\cosh k_m h \cosh k_f h - 1) - k_f h \sinh k_m h \sinh k_f h}{k_m h (1 + l/h) (k_m^2 h^2 - k_f^2 h^2)} \quad (2.35f)$$

and

$$\beta' = \begin{cases} 1 & \text{for } l \geq 0 \\ \cosh k_f l & \text{for } l \leq 0 \end{cases} \quad (2.35g)$$

$$\delta_1 = \begin{cases} 0 & \text{for } l \geq 0 \\ \sinh(k_m + k_f)l & \text{for } l \leq 0 \end{cases} \quad (2.35h)$$

$$\delta_2 = \begin{cases} 0 & \text{for } l \geq 0 \\ \sinh(k_m - k_f)l & \text{for } l \leq 0 \end{cases} \quad (2.23i)$$

$$\gamma_1 = \begin{cases} 1 & \text{for } l \geq 0 \\ \cosh(k_m + k_f)l - (k_m h + k_f h)(1 + l/h) \sinh(k_m + k_f)l & \text{for } l \leq 0 \end{cases} \quad (2.23j)$$

$$\gamma_2 = \begin{cases} 1 & \text{for } l \geq 0 \\ \cosh(k_m - k_f)l - (k_m h - k_f h)(1 + l/h) \sinh(k_m - k_f)l & \text{for } l \leq 0 \end{cases} \quad (2.23k)$$

The first-order transfer function, $T^{(1)}$ (Biésel, 1951), between the wave amplitude and the paddle displacement is given by:

$$T_m^{(1)} = a_m / X_m = \frac{2 \sinh k_m h (k_m h (1 + l/h) \sinh k_m h - \cosh k_m h + \beta)}{k_m h (1 + l/h) (\sinh k_m h \cosh k_m h + k_m h)} \quad (2.36a)$$

in which

$$\beta = \begin{cases} 1 & \text{for } l \geq 0 \\ \cosh k_m l & \text{for } l \leq 0 \end{cases} \quad (2.36b)$$

For actual calculations, the above equations are applied with subscript n as well as m to allow the principle of summation to be applied. Figure 2.7 shows the function $F_l h$ plotted versus h / L_0 for several values of f_n / f_m . The curve for $f_n / f_m = 1.0$ depicts the function values for the self-self interaction of a regular wave.

Lastly, the function F_{23} is associated with the local disturbances described by Biésel (1951). These disturbances are caused by the horizontal velocity profile mismatch between natural waves and those produced by a planar wave paddle. The disturbances experience exponential decay with distance from the waveboard and would seem rather insignificant for practical testing purposes because of their rapid decay. However, progressive, non-decaying free waves of frequency ω_Σ appear as a result of these local disturbances. Therefore, this effect must not be excluded. Recalling from Equation (2.31b) that

$$F_{23} = F_2 (F_{3,m} + F_{3,n}),$$

the components of the F_{23} function are described in dimensionless form as (Sand and Mansard, 1986a):

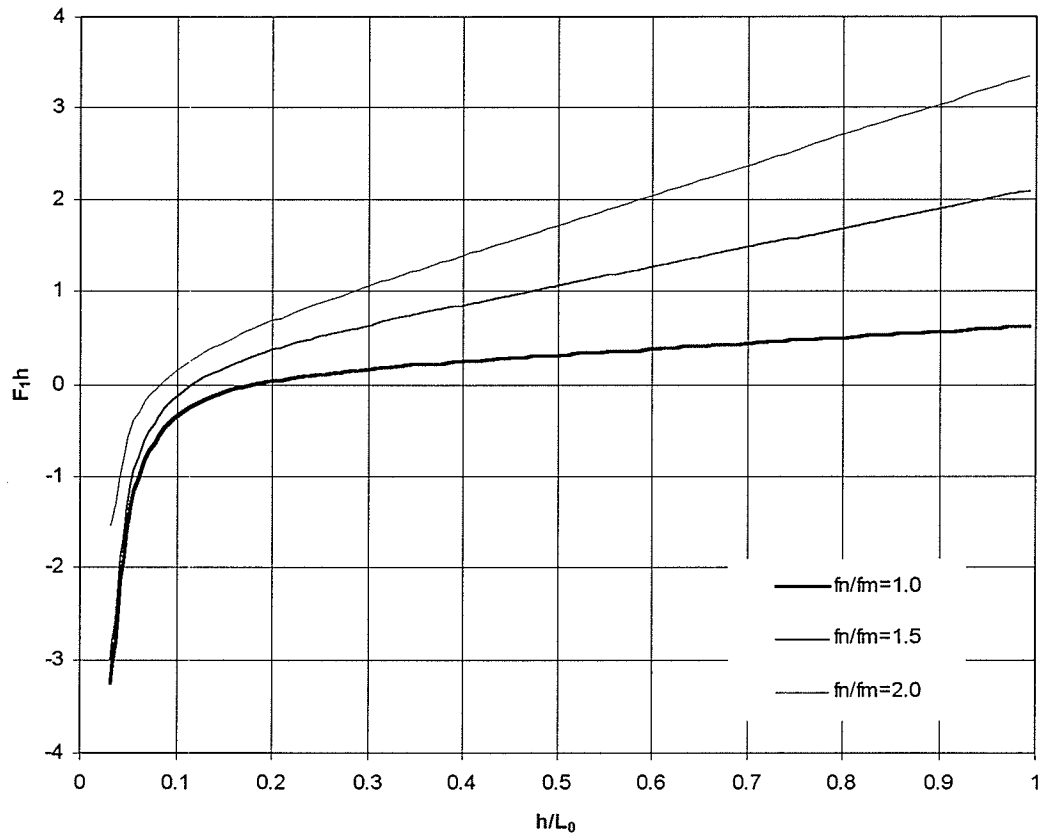


Figure 2.7 Short wave transfer function F_1h for a pair of wave components f_n and f_m as a function of h/L_0 .

$$F_2 h = \frac{k_f^2 h^2}{T_n^{(1)} T_m^{(1)} (k_f (h+l) \tanh k_f h - 1 + \beta' / \cosh k_f h)} \quad (2.37)$$

$$F_{3,m} = \frac{f_m}{f_n + f_m} \sum_{j=1}^{\infty} \frac{\cosh k_j h (k_j (h+l) \sinh k_j h + \cosh k_j h - \lambda)}{(k_j^2 h^2 + k_f^2 h^2) k_j (h+l) (\sinh k_j h \cosh k_j h + k_j h)} \\ \left[k_j (h+l) (k_f h \tanh k_f h + k_j h \tan k_j h) + k_f h \tanh k_f h \tan k_j h - k_j h \right. \\ \left. + \frac{k_j h}{k_j^2 h^2 + k_f^2 h^2} (k_j^2 h^2 - k_f^2 h^2 - 2k_f h \tanh k_f h) k_j h \tan k_j h \Omega_3 \right] \quad (2.38a)$$

in which

$$\lambda = \begin{cases} 1 & \text{for } l \geq 0 \\ \cos k_j l & \text{for } l \leq 0 \end{cases} \quad (2.38b)$$

$$\Omega_3 = \begin{cases} \frac{-k_j h (k_j^2 h^2 - k_f^2 h^2)}{(k_j^2 h^2 + k_f^2 h^2) \cos k_j h \cosh k_f h} & \text{for } l \geq 0 \\ 2k_j^2 h^2 k_f h \sin k_j l \sinh k_f l - \frac{k_j h (k_j^2 h^2 - k_f^2 h^2) \cos k_j l \cosh k_f l}{(k_j^2 h^2 + k_f^2 h^2) \cos k_j h \cosh k_f h} & \text{for } l \leq 0 \end{cases} \quad (2.38c)$$

and

$$k_j h \text{ is the real root of } \omega_m^2 h / g = -k_j h \tan k_j h, \text{ for } (j-1/2)\pi < k_j h < j\pi. \quad (2.38d)$$

The dimensionless function $F_{23} h$ is plotted in Figure 2.8 versus h / L_0 for several values of f_n / f_m . The curve depicting an f_n / f_m value of 1.0 shows the self-self interactions of a regular wave.

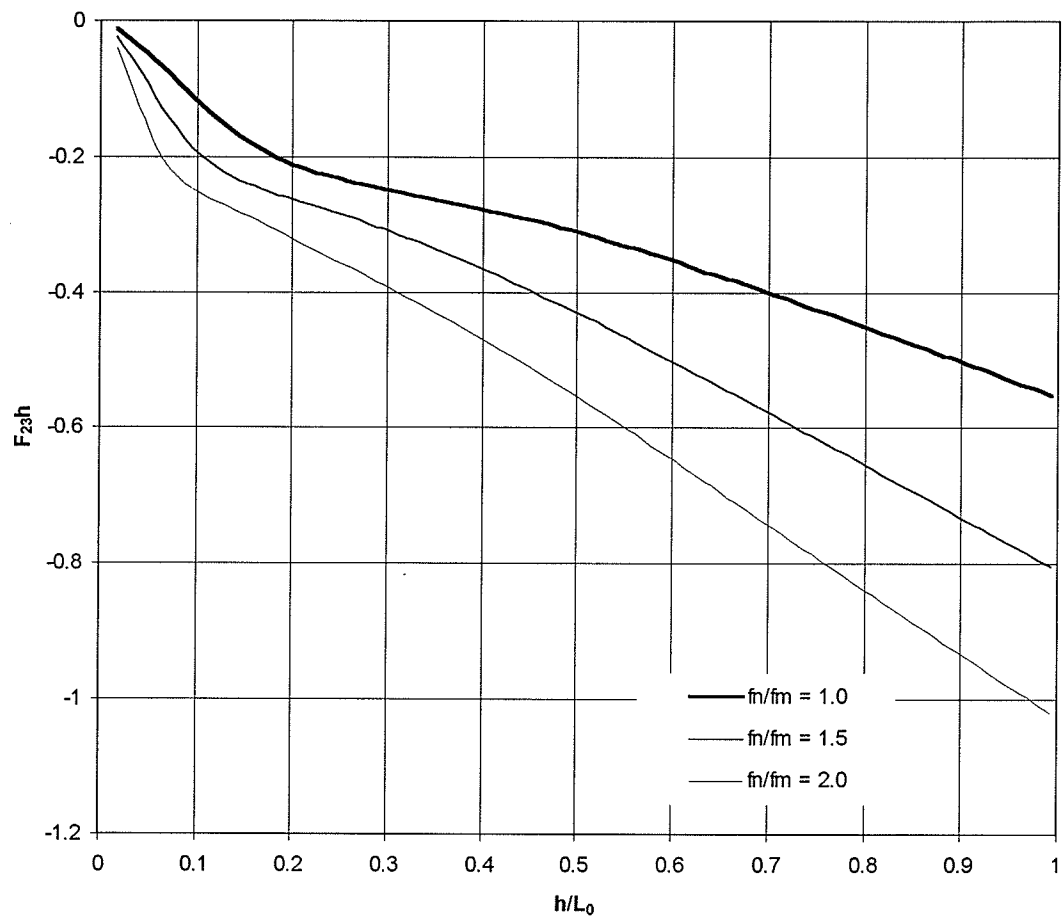


Figure 2.8 Short wave transfer function $F_{23}h$ for a pair of wave components f_n and f_m as a function of h/L_0 .

The complete second-order short wave correction signal is given as

$$X^{(2)}(t) = \sum_{n=1}^{N-1} \sum_{m=n+1}^N \left((a_n b_m + a_m b_n) F_1 + (a_n a_m - b_n b_m) F_{23} \right) \cos(\omega_\Sigma t) - \left((a_n a_m - b_n b_m) F_1 - (a_n b_m + a_m b_n) F_{23} \right) \sin(\omega_\Sigma t) \quad (2.39)$$

Chapter 3: Wave Generation Software

3.1. General Overview.

The algorithms presented in chapter 2 were coded into an interactive software package using MATLAB[®]. The use of MATLAB as the environment for a wave generation package has several benefits over using a traditional programming language. The basic data element in MATLAB is a matrix that does not require dimensioning. Any operation performed on an array is completed as a single operation rather than on an element by element basis in a loop as is typical of other programming languages. MATLAB is also capable of working with complex variables using its built-in functions to perform complex operations, such as conjugation. In addition, MATLAB's visualization (*i.e.*, plotting) capabilities are such that no other presentation software is needed to display numerical and experimental results.

The full second-order laboratory wave generation package, entitled WAVGEN, consists of one controlling script file that calls other function files as specified by the user. The first function called by the program produces a first-order wavetrain. The user may select one of three idealized spectra from which an amplitude vector is derived. Random phase angles are added to the amplitudes to produce a random wavetrain. Regular waves and bichromatic wave groups can also be specified. The function returns a first-order waveboard position vector to the controlling script file.

The user may opt for second-order long wave corrections to the first-order wavetrain which occur in a WAVGEN function call. The algorithms used to calculate the long wave corrections for a piston type wave generator are given in § 2.3.

Selecting second-order short wave corrections to the first-order wavetrain leads to another WAVGEN function call. The algorithms used to calculate the short wave corrections are found in § 2.4. The end result is a waveboard position vector correct to second-order that eliminates the spurious long and short waves inherent with a first-order control signal.

The final function call in most instances converts the waveboard position to a voltage that determines the piston displacement and does the post-processing chores before the file is sent to the wavemaker. Compensation is made for the waveboard dynamics and the wave machine servo dynamics. The post-processing module offsets the displacement array to center the waveboard motion and manipulates the data so that the waveboard starts and ends near the central position to avoid start-up transients. An optional gain factor may be applied to the array. The output is limited to +/- 10 volts. Finally, the array can be resampled at a higher frequency so that the signal sent to the wavemaker results in a smoother board motion without affecting the spectral characteristics of the wavetrain.

3.2. First-Order Wave Generation.

The first-order wave function of the WAVGEN wave generation software package produces a piston position time series based on user selected input parameters as seen in

the flowchart in Figure 3.1. Three idealized wave spectra (JONSWAP, Donelan TMA) are included in the current version of the software. Other spectral forms (Pierson-Moskowitz, Ochi, *etc.*) can be readily added.

The JONSWAP spectrum (Hasselmann *et al.*, 1973) is given by

$$S_J(f) = \frac{\alpha g^2}{(2\pi)^4 f^5} \exp\left[-\left(\frac{f_p}{f}\right)^4\right] \gamma^{\exp\left\{-\frac{(f-f_p)^2}{2\mu^2 f_p^2}\right\}} \quad (3.1a)$$

where

$$\alpha = 0.076 \left(\frac{gF}{U_{10}^2}\right)^{-0.22} \quad (3.1b)$$

$$\gamma = 3.3 \quad (\text{may vary from 1 to 7}) \quad (3.1c)$$

$$\begin{aligned} \mu &= 0.07 & f \leq f_p \\ &= 0.09 & f > f_p \end{aligned} \quad (3.1d)$$

F is the fetch length, U_{10} is the wind speed measured at 10 metres above the water surface, and γ is the peak enhancement factor. The Donelan spectrum (Donelan *et al.*, 1985) differs from the JONSWAP in the slope of the high frequency portion of the spectrum. Donelan *et al.* (1985) determined that an f^{-4} slope was more consistent with observed natural wave spectra than the JONSWAP f^{-5} slope. The Donelan spectral form is

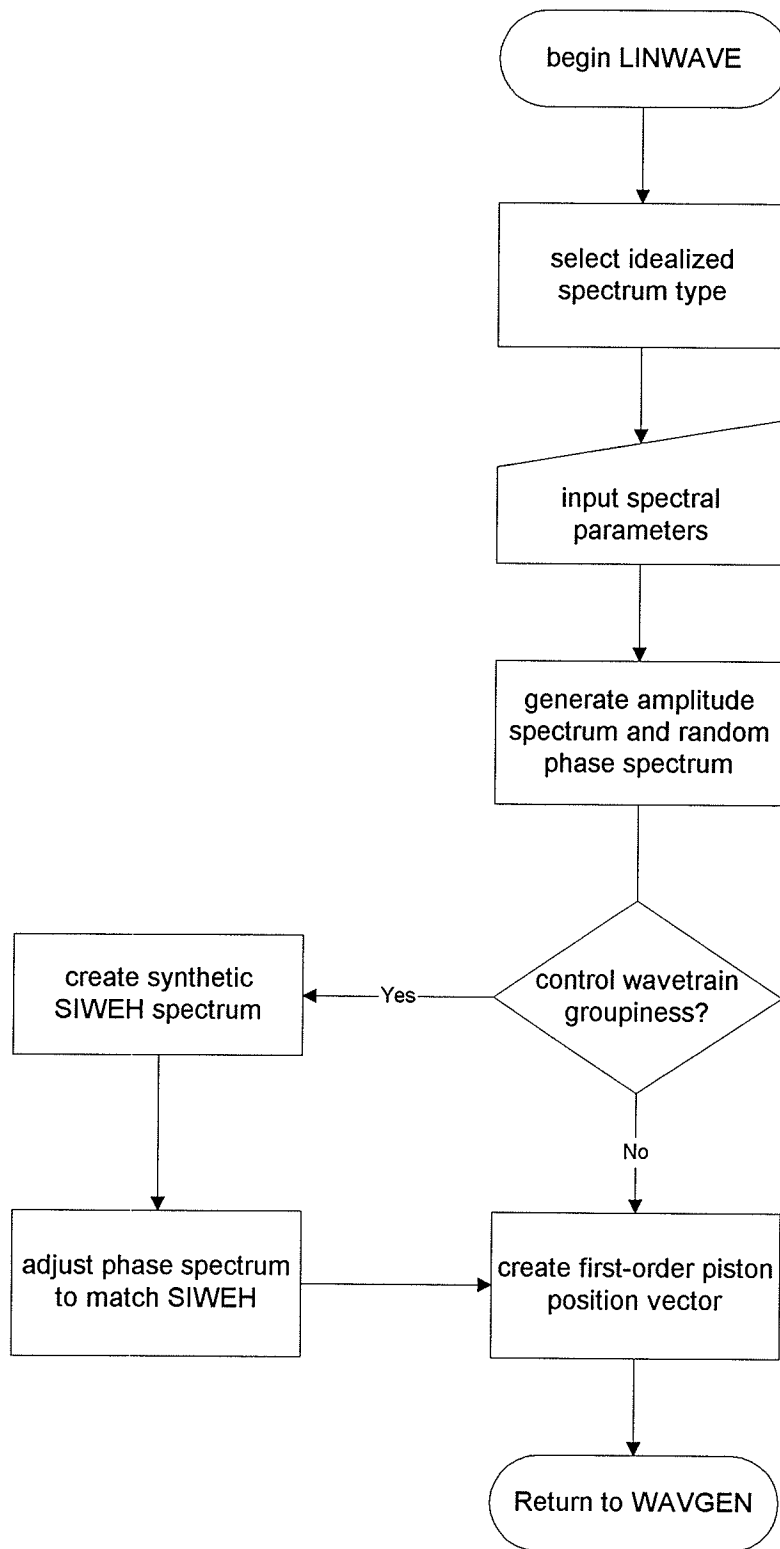


Figure 3.1 Flow chart of LINWAVE first-order wave generator function in WAVGEN.

$$S_D(f) = \frac{\alpha g^2}{(2\pi)^4 f^4 f_p} \exp\left\{-\left(\frac{f_p}{f}\right)^4\right\} \gamma^{\exp\left\{-\frac{(f-f_p)^2}{2\mu^2 f_p^2}\right\}} \quad (3.2a)$$

where

$$\alpha = 0.006 W^{0.55} \quad (3.2b)$$

$$\mu = 0.08(1 + 4W^3) \quad (3.2c)$$

$$\begin{aligned} \gamma &= 1.7 - 6.0 \log W & 0.2 < W \leq 1.0 \\ &= 1.7 & 1.0 < W \leq 1.2 \end{aligned} \quad (3.2d)$$

W is the wave age parameter defined as the ratio of the wave celerity of the peak spectral frequency, f_p , to the wind speed component in the direction of travel of the peak waves.

The TMA spectrum (Bouws *et al.*, 1985) does not assume deep water conditions at the point of wave generation making it more suitable for intermediate and shallow water laboratory wave generation than either the JONSWAP or Donelan spectrum. The TMA spectrum, which is conceptually a shoaled JONSWAP spectrum, is given by

$$S_{TMA}(f) = \frac{\alpha g^2}{(2\pi)^4 f^5} \exp\left\{-\left(\frac{f_p}{f}\right)^4\right\} \gamma^{\exp\left\{-\frac{(f-f_p)^2}{2\mu^2 f_p^2}\right\}} \phi_{TMA} \quad (3.3a)$$

where

$$\begin{aligned} \phi_{TMA} &= 0.5 \omega_h^2 & \text{for } \omega_h \leq 1 \\ &= 1 - 0.5(2 - \omega_h)^2 & \text{for } 1 < \omega_h \leq 2 \\ &= 1 & \text{for } \omega_h > 2 \end{aligned} \quad (3.3b)$$

and

$$\omega_h = 2\pi f \sqrt{\frac{h}{g}} \quad (3.3c)$$

Figure 3.2 shows the shape of the three idealized spectra included in the WAVGEN software package for a 256 second wavetrain with 4 Hz sampling and a peak period of 2 seconds. The water depth for the TMA spectrum was set to 1 m. All spectra are for fully developed wave conditions (*i.e.*, $\gamma = 3.3$, $W = 0.83$). Since the area under each spectrum is proportional to the wave height, the fully developed JONSWAP spectrum yields a larger (deep water) wave height than the Donelan spectrum. The shoaled TMA spectrum yields a considerably smaller wave height than either the JONSWAP or Donelan spectrum.

The user is required to provide values for the necessary spectral peak enhancement factors as well as the overall length of the record to be produced, the sampling frequency, and the peak frequency of the linear waves. Random phase angles are applied to each frequency to convert the spectral ordinates into complex Fourier coefficients. The random number generator seed value can be specified to facilitate comparisons over multiple runs. The groupiness of the wave record is controlled using the Synthetic Instantaneous Wave Energy History (SIWEH) approach of Funke & Mansard (1979). The SIWEH algorithm was coded and tested by Baryla (1996). The user is presented with a plot of the time series in both the time and frequency domains at the conclusion of the function as shown in Figure 3.3. The function returns a waveboard position time series to the controlling script file.

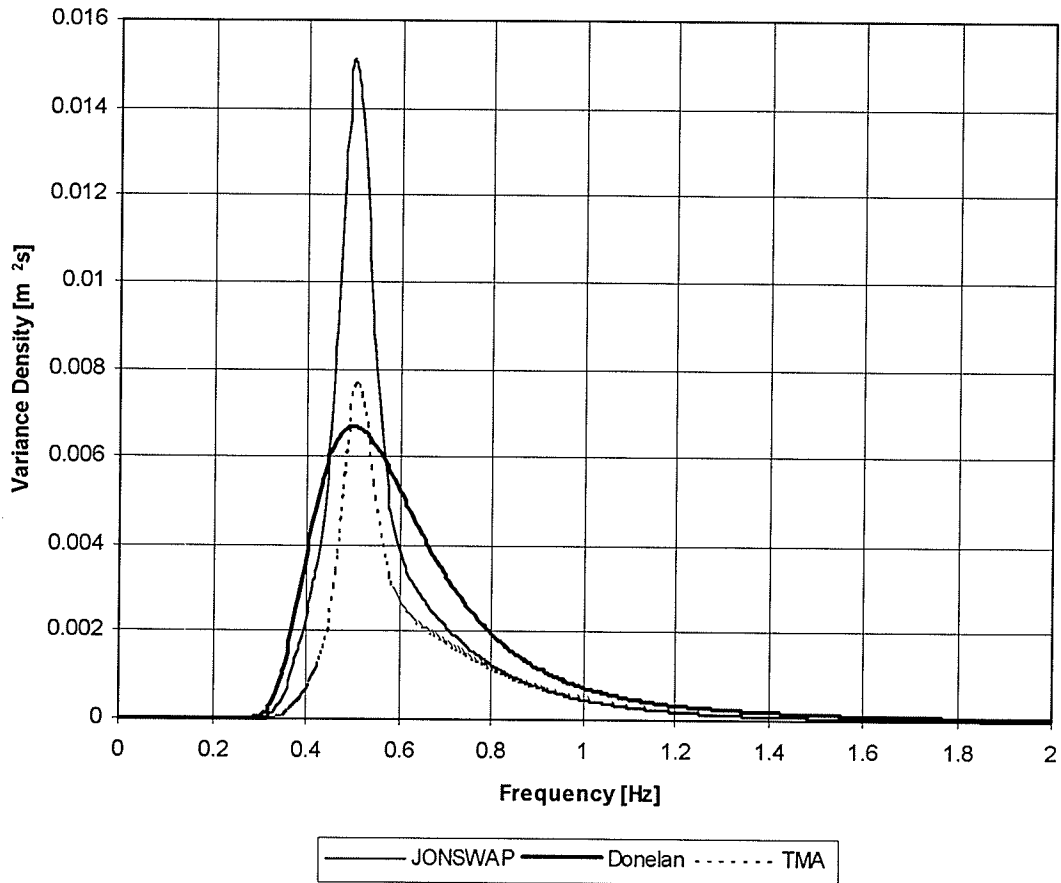


Figure 3.2 Idealized spectra used in LINWAVE first-order wave generator in WAVGEN.

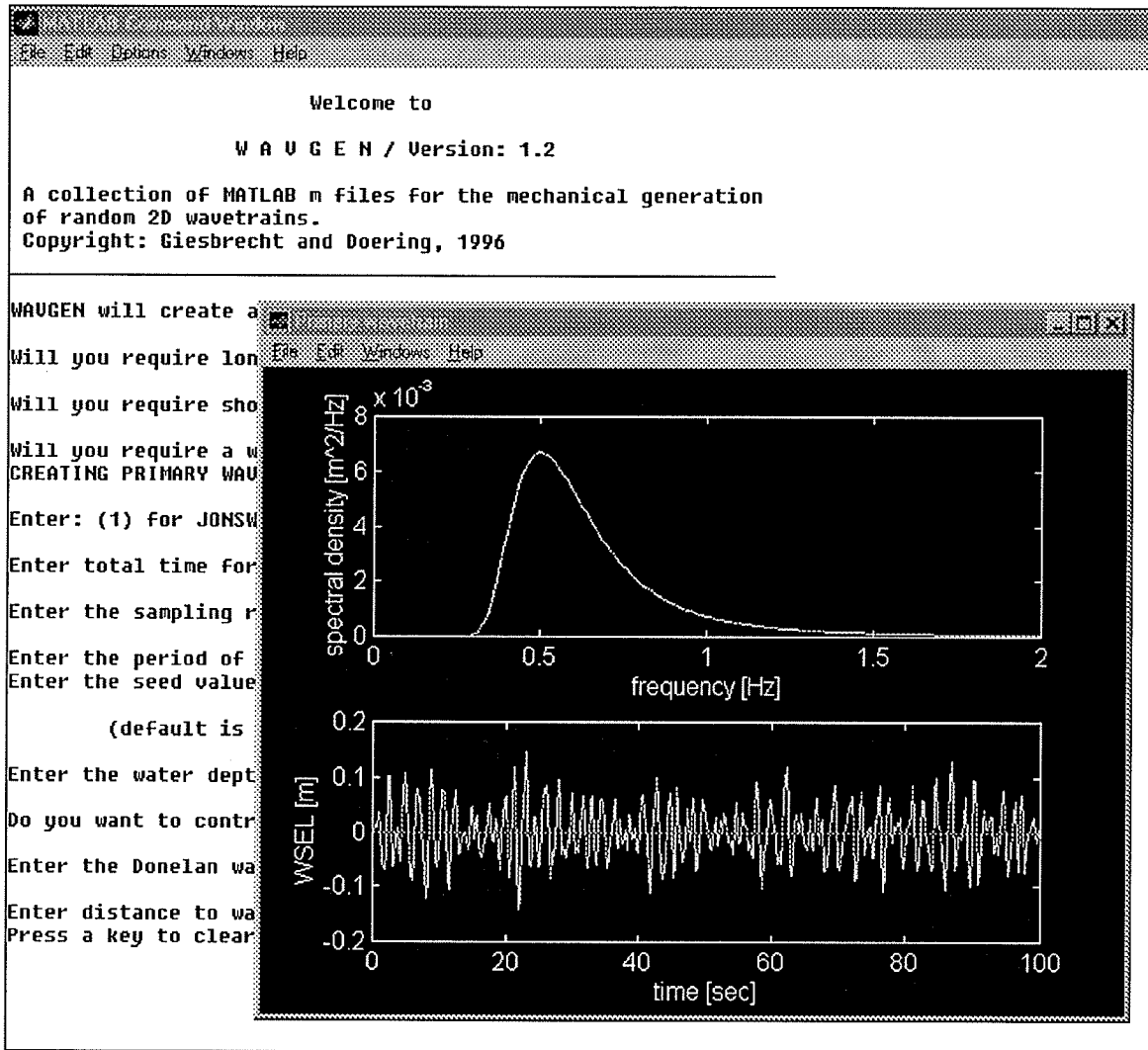


Figure 3.3 WAVGEN first-order wave train generation display screen.

3.3. Threshold Limited Approach.

Computing the desired second-order corrections for an irregular wavetrain by straightforward summation is tedious and time consuming due to the single infinite series involved in the calculation of the local disturbance waves (see Equations (2.29a) and (2.38a)). A threshold limited approach is proposed here to facilitate quicker calculation of the correction factors by applying the corrections to the frequencies that are most affected by them.

The threshold limited approach to second-order corrections makes use of the knowledge that for many frequencies, the long or short wave correction is negligible as the amplitude of frequencies away from the peak is quite small. The long wave corrections are significant only at the lower frequencies of the wave spectrum, therefore they need not be calculated over the rest of the spectrum. The threshold cut-off is a user specified percentage of the power in the spectral peak. The computations are performed only for those frequencies whose power is less than the threshold value and are limited logically to the lower portion of the spectrum even though some frequencies in the upper reaches of the spectrum also meet the threshold criterion. The full frequency space is used in the calculation of the long wave corrections but only for the frequency differences that fall within the threshold limited range.

For the short wave corrections, only the frequencies near the first and second harmonics of the spectral peak experience a significant correction due to the presence of short waves. The threshold cut-off in this instance defines the range of frequencies that will be used in

the calculation of these short wave corrections. All frequencies whose power exceeds the threshold limit are considered. The corrections are applied to all possible frequency sums up to and including the Nyquist frequency. All frequency sums higher than the Nyquist frequency are not physically reproducible and thus are not considered.

The accuracy of the approximation can be varied by changing the cut-off to a higher or lower percentage of the peak spectral power. Comparisons can readily be made to a base case that includes corrections to the entire spectrum for both the long and short waves.

3.4. Long Wave Correction.

The long wave correction function of WAVGEN incorporates the threshold limited approach described above to improve algorithm efficiency. The algorithm used is presented in section 2.3 and was subsequently coded into a set of MATLAB function files that operate according to Figure 3.4. The threshold limit is specified by the user as a percentage of the variance density in the peak frequency. This percentage is multiplied by the peak variance density to yield the upper limit for the correction calculations. Only the low frequencies whose variance density falls below the threshold value calculated have corrections calculated for them. Figure 3.5 illustrates the thresholding technique for the case of long wave corrections. With the 10% threshold indicated, only those frequency differences lower than 0.4 Hz will have a correction calculated. The peakedness of the spectrum enables us to set the threshold quite low resulting in a much faster calculation without sacrificing a great deal of accuracy. The correction factors F_{11} and F_{12} are calculated in order to eliminate the free parasitic wave and the displacement wave, while

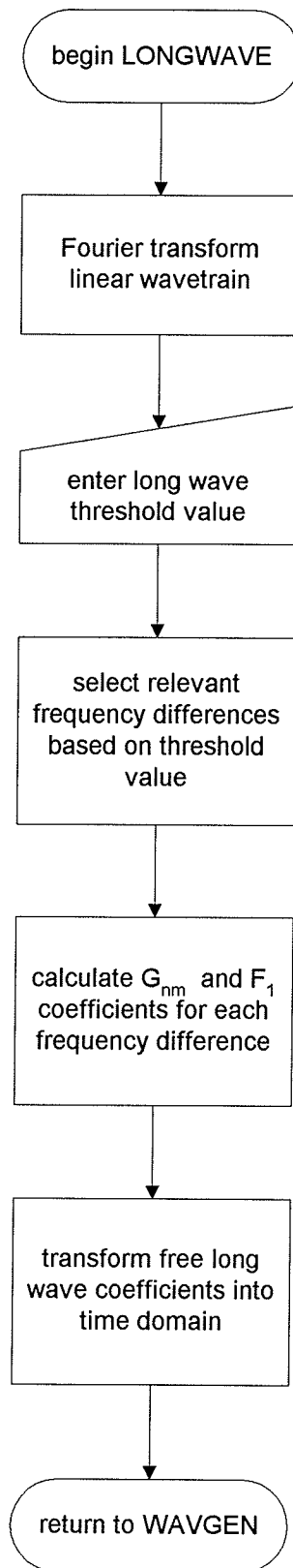


Figure 3.4 Flow chart of LONGWAVE second-order long wave correction function in WAVGEN.

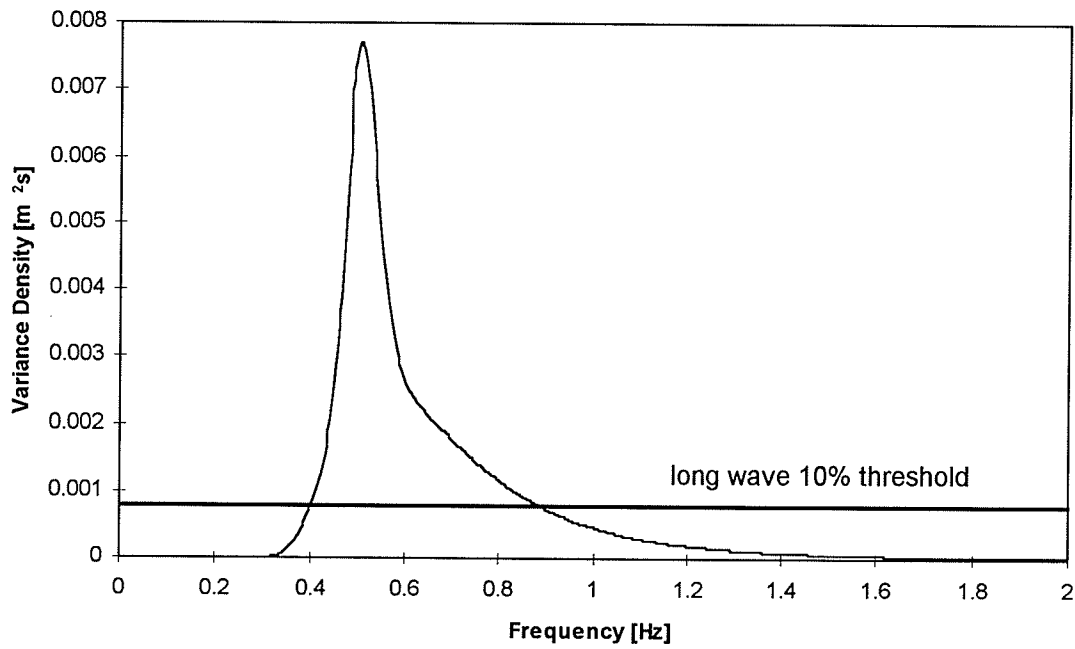


Figure 3.5 Long wave threshold of 10% applied to a fully developed TMA spectrum, 1 m water depth, sampled at 4 Hz, $f_p = 0.5$ Hz.

F_{23} which is related to the evanescent wave is omitted as described in chapter 2. The long wave correction function results in a second-order waveboard position series that represents the spurious waves generated by a first-order control signal. This time series is then subtracted from the first-order waveboard position record.

The prototype random wave record used in the threshold analysis was based on a fully developed TMA spectrum, 600 seconds in length, sampled at 4 Hz, with a peak frequency, f_p , of 0.5 Hz. Although the following analysis is numerical, this wave record is typical of those used in physical testing in the HRTF random wave flume and indicates the extent and duration of the correction calculations that can typically be expected. Using the TMA spectrum accounts for any shoaling that needs to occur to correctly place this wavetrain in the 1 m depth of water found in the wave flume. Figure 3.6 shows the relative times to complete the threshold limited long wave correction calculations based on the time to fully correct the wave record. The greatest improvement in the time to calculate the long wave corrections is 22%, indicating that the algorithm does not spend much of its time in calculating the corrections. The actual time for full correction using a 486/DX66 with 12 megabytes of RAM was 537 seconds (8.9 minutes) for long waves. Figure 3.7, panels a-c, shows the long wave correction piston position series for threshold values of 100% (full correction), 10% and 5%, respectively. There is a slight loss of amplitude as the threshold value decreases and fewer frequencies are corrected for spurious long wave effects, however, little of the detail in the correction is sacrificed.

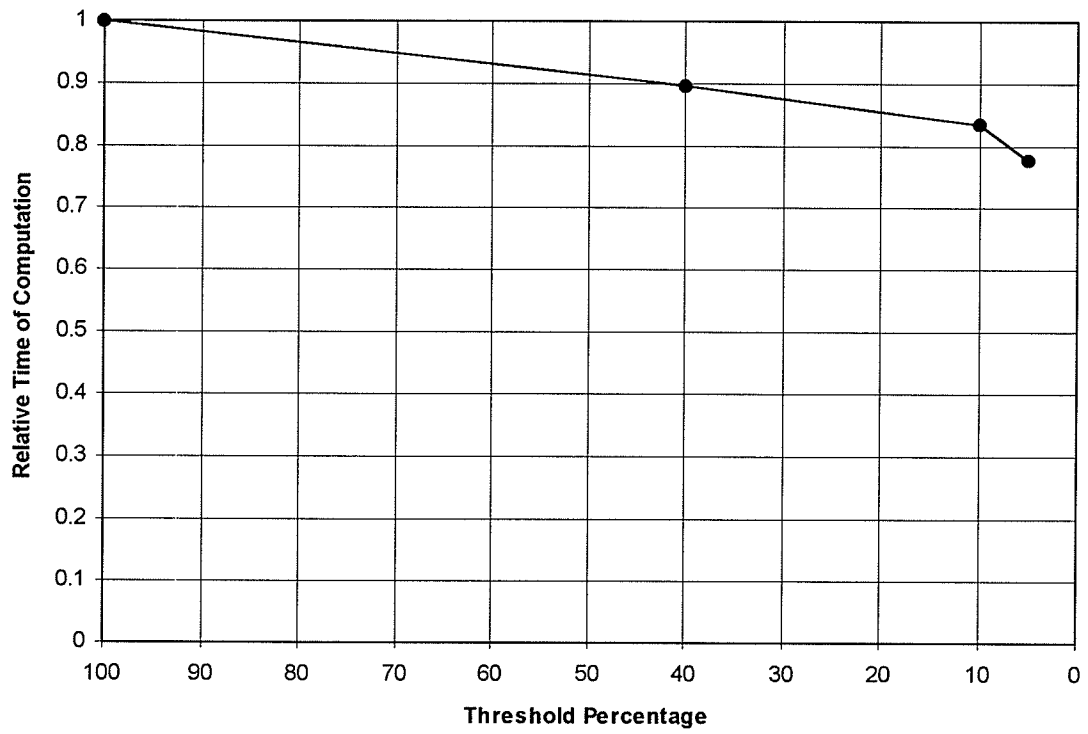


Figure 3.6 Second-order long wave correction computational effort as a function of threshold value.

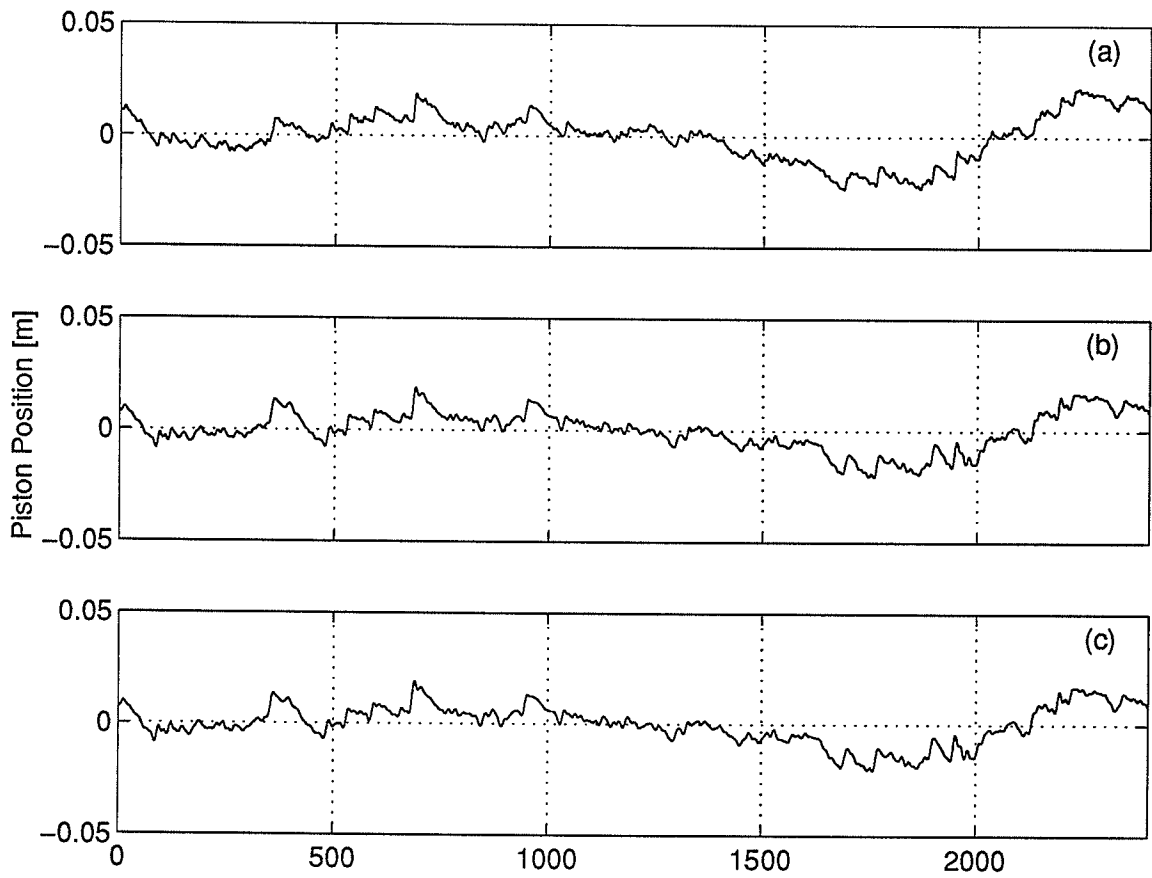


Figure 3.7 Long wave correction piston position signals for threshold values of (a) 100% (full correction); (b) 10% and; (c) 5% applied to fully developed TMA spectrum, 1 m water depth, sampled at 4 Hz, $f_p = 0.5$ Hz.

3.5. Short Wave Correction.

The short wave correction function in WAVGEN, illustrated in Figure 3.8, includes the threshold limited approach to improve algorithm efficiency. It is of greater utility in this case than for the long wave corrections because of the infinite series that occur in the calculation of the evanescent wave amplitude ratio, F_{23} (Equation 2.26). In this case the threshold value calculated results in the lower limit for the primary frequencies to be included in the short wave corrections. This limits the frequencies used in the calculation to those near the spectral peak where the majority of the variance density resides. Figure 3.9 shows the use of thresholding in limiting the number of frequencies used in the short wave corrections. With a 70% threshold as indicated, only the energy between the frequencies of 0.45 Hz and 0.55 Hz are used to calculate the second-order short wave corrections. Clearly even a low threshold percentage will reduce the computational effort by a significant amount given the narrow peak of the spectrum. The short wave correction function calculates values for F_{11} , F_{12} , and F_{23} (see § 2.3) to find the amplitudes of the spurious free parasitic wave, displacement wave, and evanescent wave produced at each sum frequency. Calculation of F_{11} and F_{12} is straightforward. The F_{23} function, consisting of F_2 , $F_{3,m}$ and $F_{3,n}$, includes the evaluation of an infinite series for each component frequency. The infinite series converges on a solution quickly, so a close convergence tolerance can be set.

The Newton-Raphson method of root finding is applied to Equation (2.38d). A matrix of solutions for all possible frequency components and sums is precalculated and used as a lookup

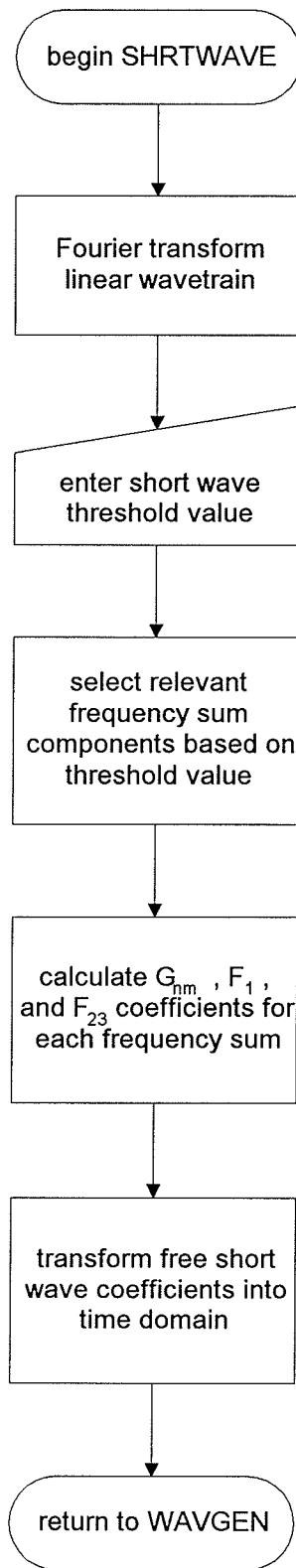


Figure 3.8 Flow chart of SHRTWAVE second-order short wave correction function in WAVGEN

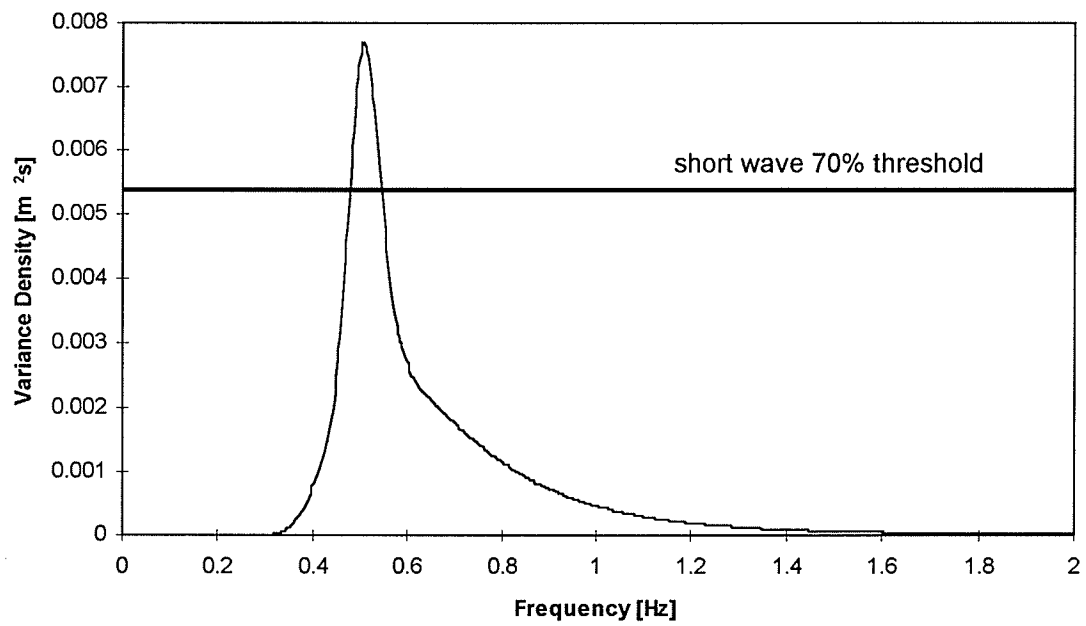


Figure 3.9 Short wave threshold of 70% applied to fully developed TMA spectrum, 1 m water depth, sampled at 4 Hz, $f_p = 0.5$ Hz.

table later in the correction function. Since the solutions to Equation (2.38d) are sensitive to the first approximation to the solution, care must be exercised in selecting the first approximation. By setting the lower bound of each interval as the first approximation to the solution, a stable solution can quickly be reached. It is quite easy to detect a problem with the convergence of the series as the time required to reach a stable solution increases dramatically.

The second-order waveboard position vector describing the spurious free waves is subtracted from the first-order waveboard position series.

Using the same prototype random wave record used in § 3.3 for the long wave analysis, Figure 3.10 shows the relative times to complete the threshold limited short wave correction calculations based on the time to fully correct the wave record. The short wave corrections benefit greatly from the use of thresholding with just a 30% threshold resulting in a reduction in computational effort by one half. The actual time for full correction using a 486/DX66 with 12 megabytes of RAM was 10877 seconds (3.02 hours). Figure 3.11 shows the calculated corrections for short wave threshold values of 1% (full correction), 10%, 30%, 50%, and 70% are seen in panels a-e, respectively. A closer examination of Figure 3.10 indicates that 1% and 10% thresholding are virtually identical. The structure of the correction changes somewhat for 30% thresholding. For increased thresholding, there is a noticeable change in the structure of the correction.

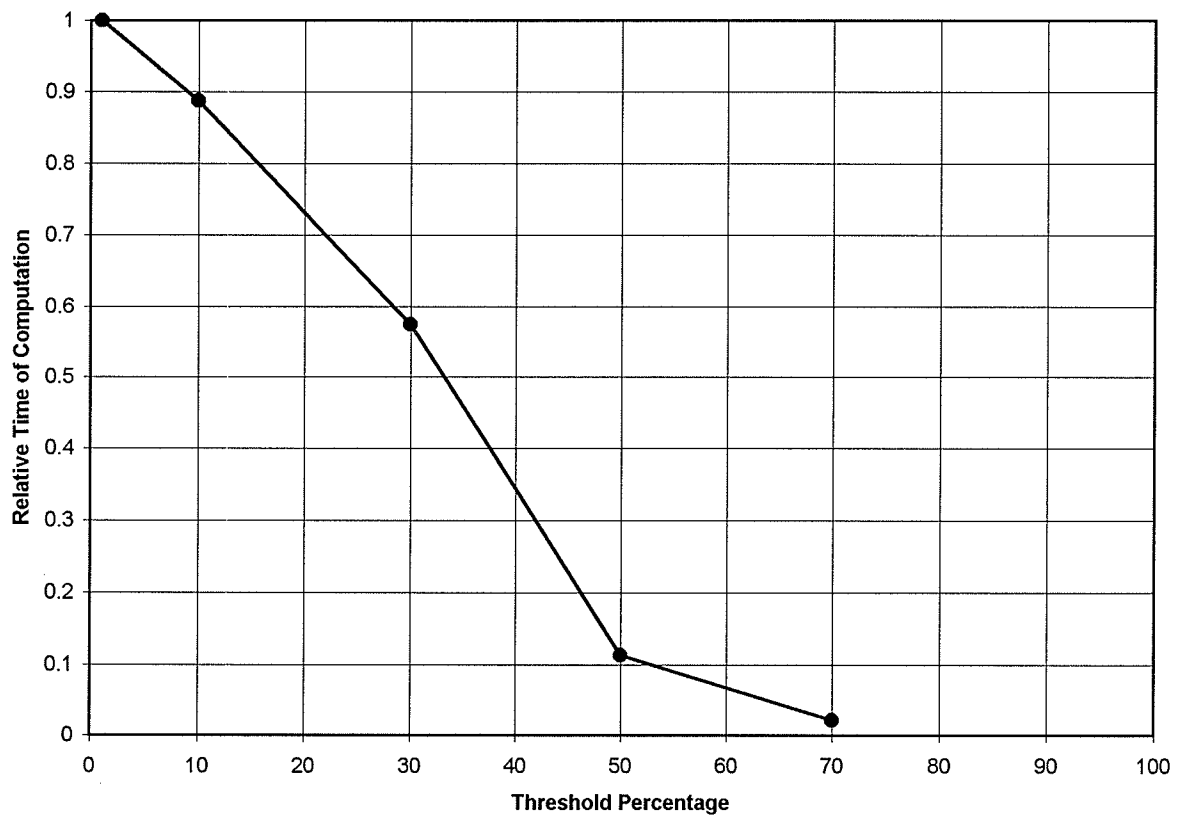


Figure 3.10 Second-order short wave correction computational effort as a function of threshold value.

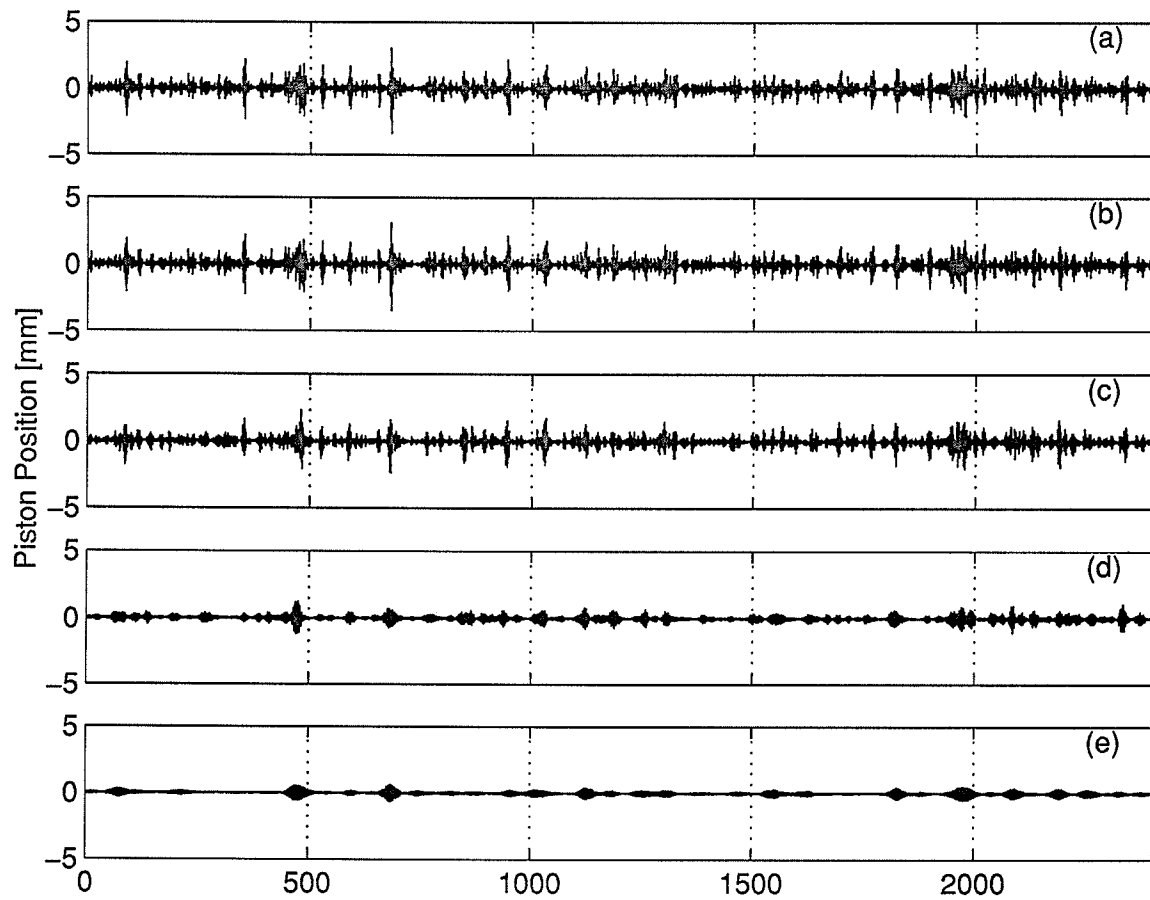


Figure 3.11 Short wave corrections piston position signal for threshold values of (a) 1% (full correction); (b) 10%; (c) 30%; (d) 50%; and (e) 70% applied to a fully developed TMA spectrum, 1 m water depth, sampled at 4 Hz, $f_p = 0.5$ Hz..

3.6. Driving Signal Creation.

The final stage in the program converts the waveboard position vector created and modified in the previous function calls into a piston position record in a form that the piston driver can understand. This function follows the algorithm laid out in Figure 3.12. The program uses machine specific values for the machine gain, voltage gain, first and second half power servo-hydraulic frequencies to convert an input waveboard position vector into a voltage series. The voltage series is then shifted such that the maximum board excursion from the mean position is equal in both directions. The beginning and end of the series are truncated such that it can readily be recycled a number of times without producing any transients. Maximum and minimum piston positions are imposed on the signal to stop the piston just shy of the physical stops with appropriate warnings to the user that the record has been significantly altered. The voltage series is then converted to a series of integer values that correspond to specific piston displacements. This series configuration is dependent on the piston length, D/A board configuration, and the control card configuration. The user can opt to resample the driving signal at a higher rate to smooth the board motion without changing the spectral characteristics of the signal. If the maximum waveboard slew rate in either direction is exceeded, potentially significant changes to the record are made to correct that and the user is warned. A sample section of the driving signal is displayed for a visual inspection by the operator. The signal can be written to a file as specified by the user, formatted to be accepted by the program used to drive the waveboard.

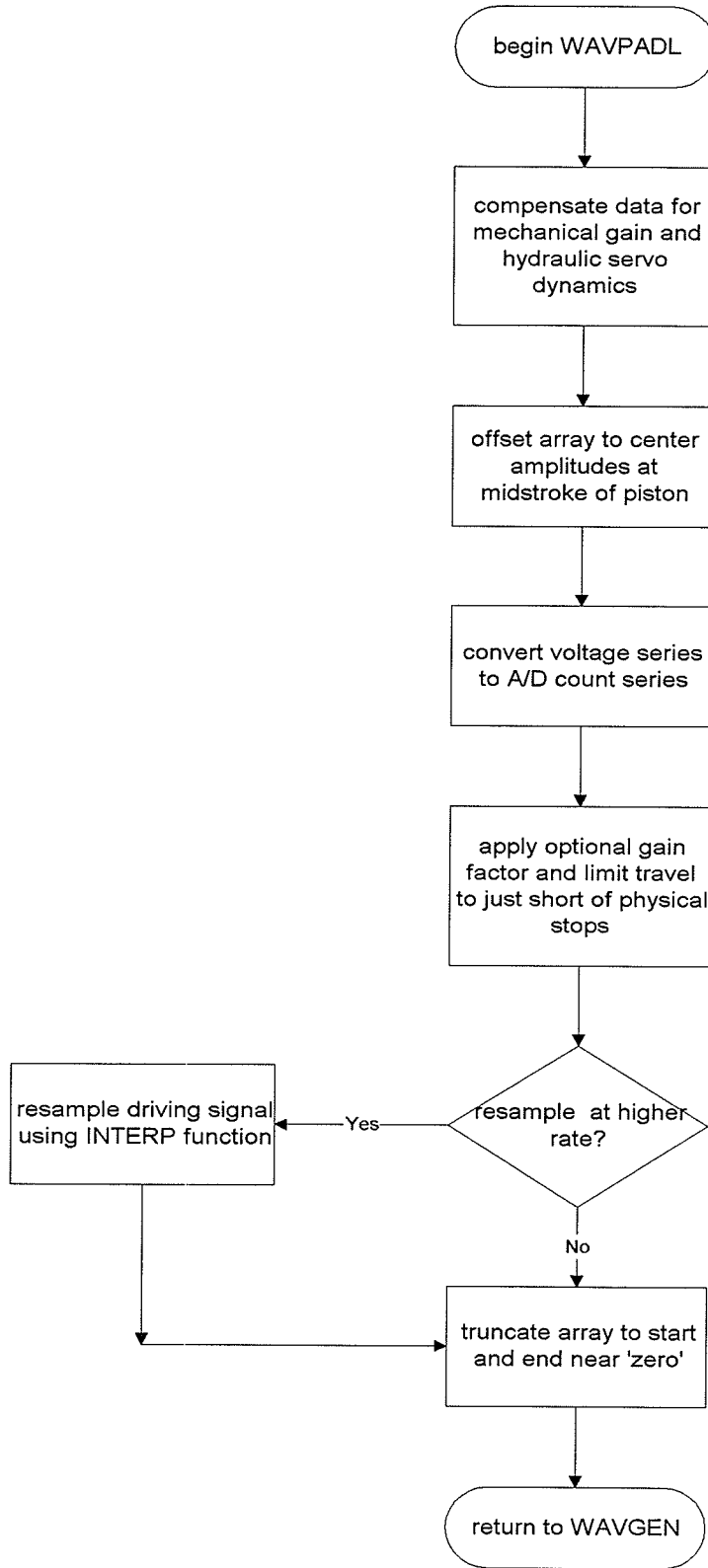


Figure 3.12 Flow chart of WAVPADL driving signal generator in WAVGEN.

Chapter 4: Physical Testing

4.1. Apparatus.

The data used for testing the veracity of the WAVGEN software package was collected in the random wave flume in the Hydraulics Research & Testing Facility (HRTF) at the University of Manitoba. This reinforced concrete flume measures 34-m long, 1.5-m wide, and 1.5-m deep. It is equipped with a hydraulically-actuated, piston-type waveboard, a system of upright wave absorbers, wave probes, and a natural sand, wave-absorbing beach initially with a 1:10 slope as shown in Figure 4.1.

The waveboard is driven by a 2-inch bore, 46-inch stroke high performance cylinder, which is powered by a 40-HP hydraulic pump capable of supplying 40 USGPM at 2500 psi. All components are manufactured by Vickers. To achieve maximum positional accuracy, a high frequency Vickers VM4-40 bipolar servovalve operates in conjunction with a Temposonics II linear displacement transducer (LDT) to provide a feedback loop. The LDT precisely senses the position of an external magnet to measure displacement with a high degree of accuracy and resolution by using the principle of magnetostriction to convert the time interval between the initiation of an interrogation pulse and the detection of a return pulse into a distance measurement.

The piston displacement series is sent to the waveboard using a Keithley-Metrabyte DAC02 digital to analog (D/A) card. The signal is subsequently sent to a Vickers EM-D-

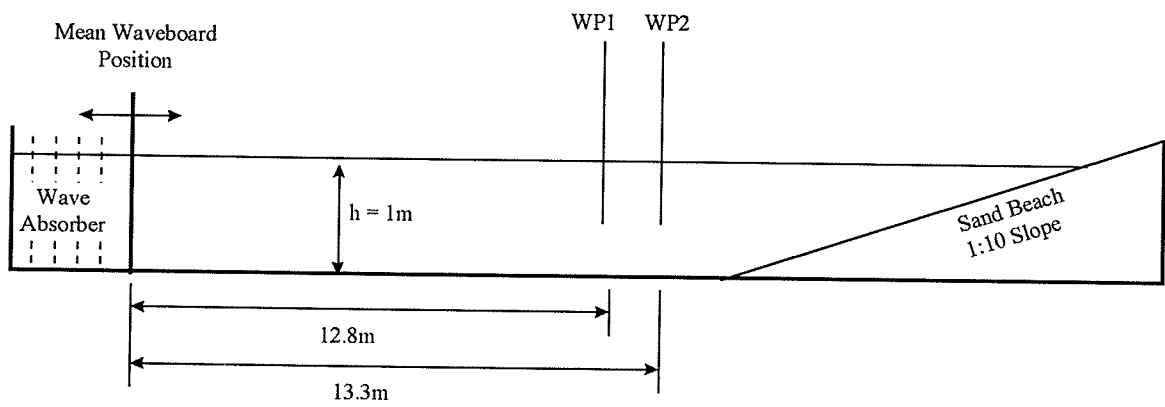


Figure 4.1 Schematic of the HRTF random wave flume used for testing WAVGEN.

30 servoamplifier with a proportional-integrating-differentiating (PID) circuit. The amplifier module sends a command signal to the SM4-40 servovalve and receives feedback from the Temposonics II LDT. The PID feedback loop was tuned to optimal performance and allows the piston to be located to within 0.25 mm of its assigned position.

Wave energy created in the flume travels away from the oscillating waveboard in the forward and reverse directions. The forward propagating wave energy is dissipated on a natural sand beach. The beach slope and configuration are allowed to change such that an equilibrium is attained with the incoming wavetrains. The sand used for the beach is very fine both to emulate the conditions found at many of the beaches in Manitoba as well as to allow scale reductions in future testing protocols. The sand gradation follows the curve shown in Figure 4.2. Wave energy propagating away from the rear face of the waveboard is dissipated by an upright wave absorber. Rear absorbers placed behind wet back generators prevent the resonance of waves that might otherwise overtop the rear wall of the flume or reflect back to the wave generator causing excess pressure on the waveboard. The design of the absorber, based on Jamieson and Mansard (1987), consists of multiple rows of perforated vertical metal sheets which progressively decrease in porosity towards the rear of the absorber. Two sheets of Expanded Metal Corp.'s $\frac{3}{4}$ "-#081LT, $\frac{1}{2}$ "-#051, and $\frac{5}{16}$ "-#051 standard expanded aluminum, with open areas of 75%, 60%, and 55%, respectively, were installed behind the waveboard in the HRTF wave flume.

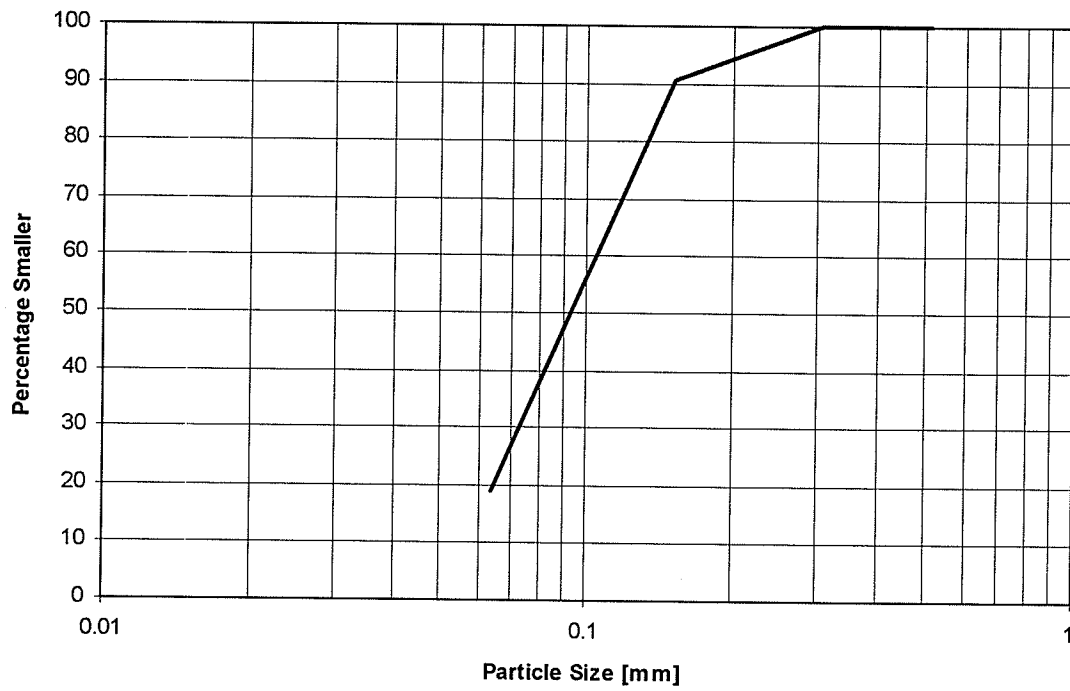


Figure 4.2 Beach sand particle size distribution (source: LSL Contracting & Materials)

Water surface fluctuation data was collected using two capacitance-type wave gauges (Model WG-30) manufactured by Richard Brancker Research Ltd. Two gauges were used to obtain information on the reflection of wave energy by the beach and on the temporal stability of the waveforms. Data acquisition from the wave gauges is handled by Labtech Notebook® software, through a Keithley-Metrabyte DAS1602 A/D card. Labtech Notebook controls the initiation, sampling rate, and termination of the data stream from each of the gauges.

4.2 Laboratory Limitations.

Great care is typically exercised in ensuring that laboratory conditions closely emulate natural conditions. However, certain inherent laboratory limitations exist that can lead to errors in the experimental results. One potential source of error is the response of the waveboard to a command signal. If the waveboard cannot perform the position changes sent to it in the time allotted (slew rate limit), then the waves produced will not be consistent with the waves desired. In a laboratory flume wave attenuation occurs due to the sidewall and bottom friction, and due to the gap around the edges of the waveboard. Reflection of wave energy off of the beach will also affect the shape of the measured waves which will include both the incident and reflected wave energy. The differences arising from the wave generating mechanism (wave paddle vs. wind) have been accounted for in the second-order correction algorithms discussed in chapter 2.

4.2.1. Waveboard Response.

Once a wavetrain is numerically created and corrected for spurious second-order effects the waveboard must be able to accurately reproduce it. If it cannot, the waves produced will be either undersized or distorted especially when long, rapid piston strokes occur. Response of the HRTF waveboard was tested using an analog function generator to create the driving signal. With a sine wave being sent to the waveboard, the frequency was increased progressively from an initial value of 0.5 Hz to 5 Hz. There was no detectable deterioration in the response of the system over the tested frequency range. Figure 4.3 shows a portion of a control signal and the associated feedback signal from the LDT. The feedback signal was consistently 10% greater than the control signal indicating that the drive signal was amplified with respect to the feedback loop. After correcting for the gain difference, the traces of the two signals are virtually identical; only a few small details ~ 1 to 2 mm in amplitude were improperly reproduced.

To further indicate the ability of the wave generator to correctly produce the desired wavetrain sent to it, it is useful to compare the target and measured primary wave spectra. Figure 4.4 shows the target spectrum (fully developed TMA spectrum, $h = 1$ m, $\Delta t = 0.25$ s, $f_p = 0.5$ Hz) and the corresponding measured wave spectrum. The two traces show clearly that the spectrum of the primary waves produced in the flume are consistent with the target spectrum selected.

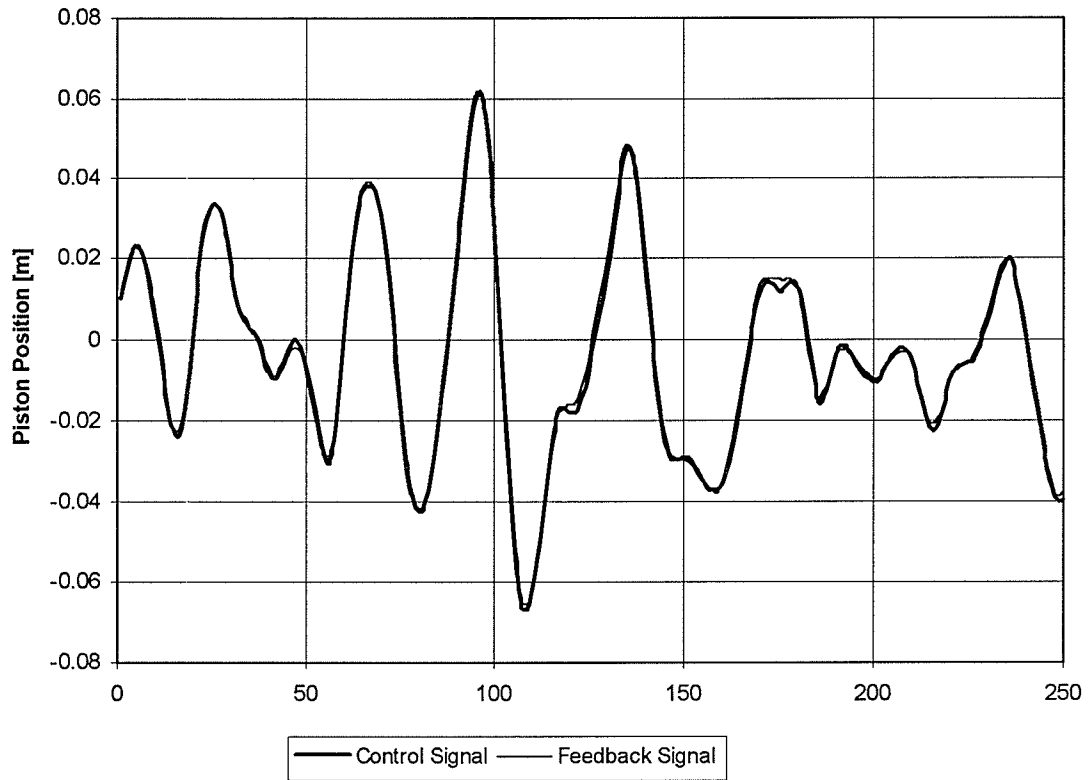


Figure 4.3 Time series of control signal and feedback signal for fully developed TMA spectrum, 1 m water depth, sampled at 4 Hz, $f_p = 0.5$ Hz.

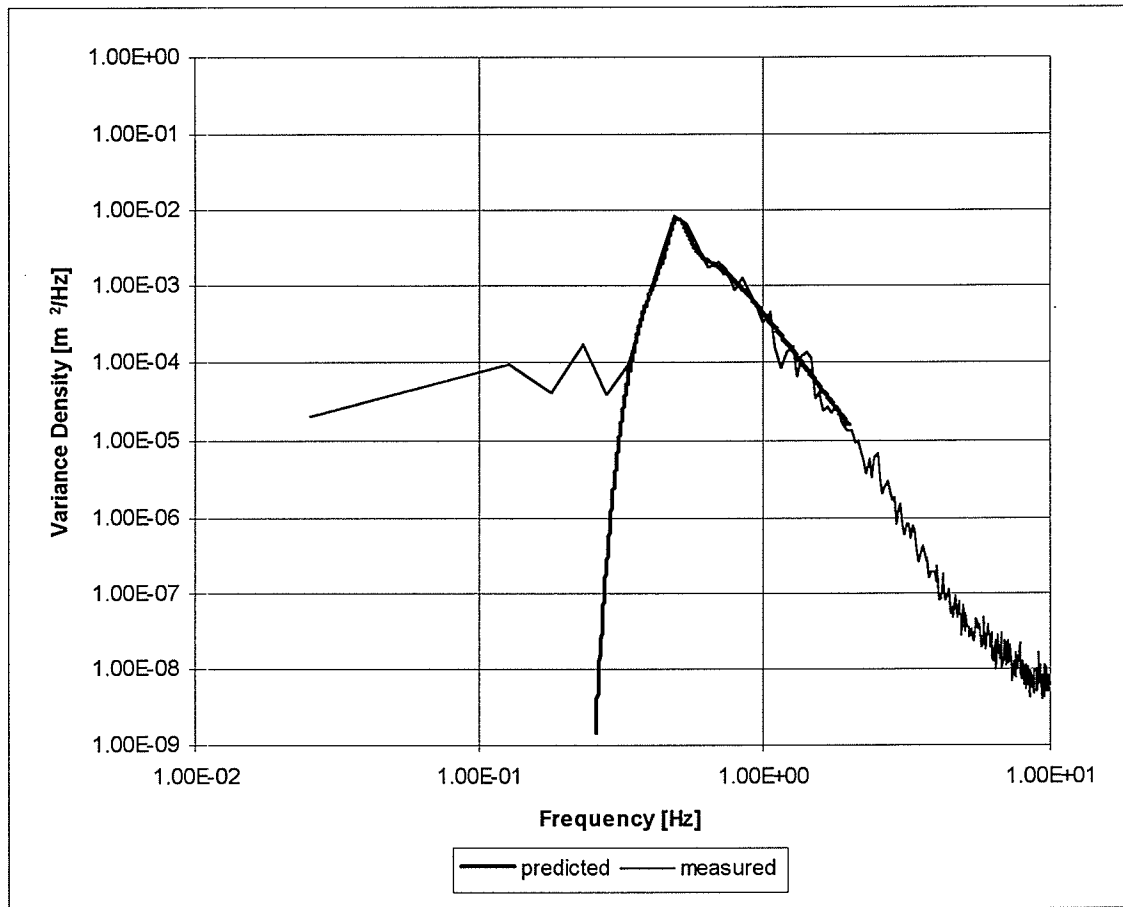


Figure 4.4 Predicted and measured spectra for a wavetrain created using a fully developed TMA spectrum, 600 seconds long, sampled at 4 Hz, in 1 m of water, with $f_p = 0.5$ Hz.

4.2.2. Wave Attenuation.

Laboratory waves attenuate with distance due to viscosity primarily in the boundary layers occurring on the sidewalls and the bottom. There is bottom friction in nature but no wall friction. Hunt (1952) gave theoretical results for the damping of amplitude for waves over an inclined bed where the slope is small. Treloar and Brebner (1970), using direct measurements of sidewall and bottom rates of energy dissipation in a flat bottomed flume, produced an adjusted formula for the wave height attenuation modulus. The wave height attenuation equation is given as:

$$\frac{H}{H_0} = e^{-\alpha x} \quad (4.1)$$

where H_0 = wave height at position $x = 0$

H = wave height at position x in the direction of propagation

α = wave height attenuation modulus

Treloar and Brebner's (1970) adjusted attenuation modulus, α_{b+w} , is given as:

$$\alpha_{b+w} = \frac{k}{B} \sqrt{\frac{T\nu}{\pi}} \left[\frac{1.48Bk + 0.94 \sinh 2kh}{2kh + \sinh 2kh} \right] \quad (4.2)$$

where B = flume width

ν = kinematic viscosity

k = wave number

T = wave period (s)

h = still water depth

For the specific case of the HRTF random wave flume filled to a still water depth of 1 m, Figure 4.5a shows the adjusted attenuation modulus for the range of frequencies from 0 to

2 Hz. The wave height attenuation ratio at the wave probes ($x = 13$ m) is illustrated in Figure 4.5b over the same frequency range. Only the highest frequencies where little of the energy of the spectrum is found experience significant attenuation. The wave height at the waveboard ($x = 0$) at these frequencies is typically on the order of millimetres. Clearly, wave attenuation due to friction can be considered negligible under the test conditions.

Wet back wave generators have a slight gap that extends around the perimeter of the waveboard between it and the sidewalls and bottom. This gap allows water to flow around the waveboard as it oscillates which attenuates the wave amplitude as it is created at the waveboard. On the forward stroke of the piston, water is piled up in front of the waveboard and the attenuation occurs as some of that water moves behind the waveboard. In a similar fashion, on the reverse stroke the water tends to pile up on the back side of the board and bleed off into the wave trough being created on the front of the board. The attenuation factor due to a gap around the perimeter of the waveboard is given by (CCIW, personal communication):

$$\alpha_{gap} = \frac{kc}{\sqrt{1 + (kc)^2}} \quad (4.3a)$$

where

$$c = \left(\frac{-2h}{\pi} \right) \ln \left(\sin \left(\frac{\pi \Delta_{gap}}{2h} \right) \right) \quad (4.3b)$$

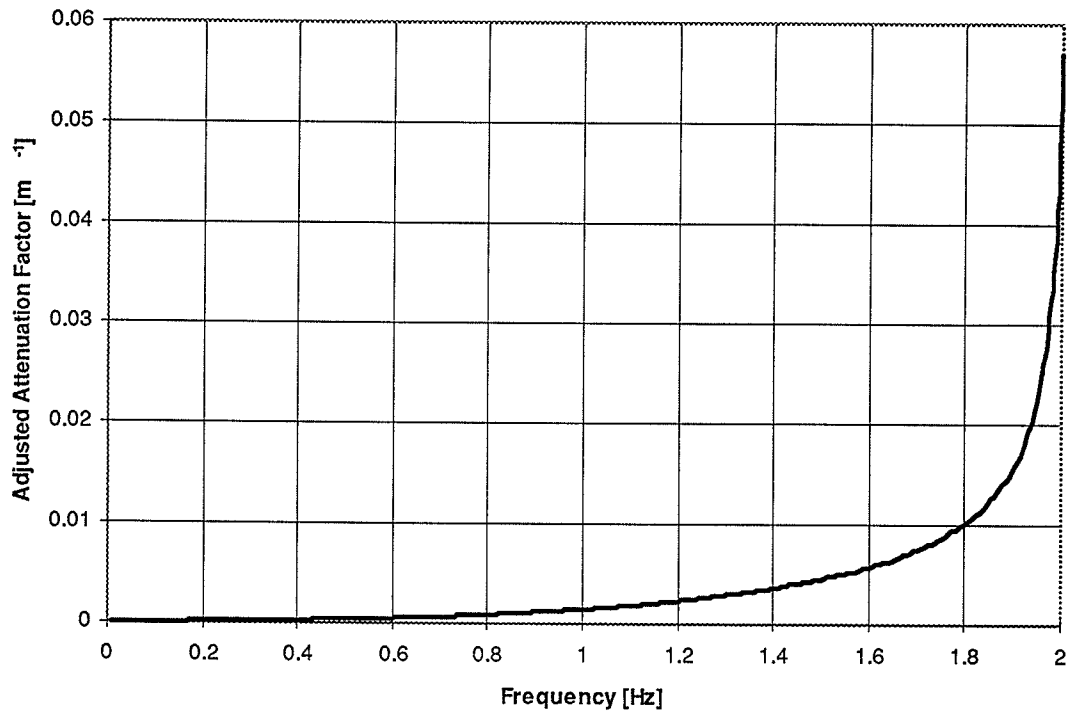


Figure 4.5a Wave height attenuation factor due to sidewall and bottom friction as a function of frequency (Treloar & Brebner, 1970).

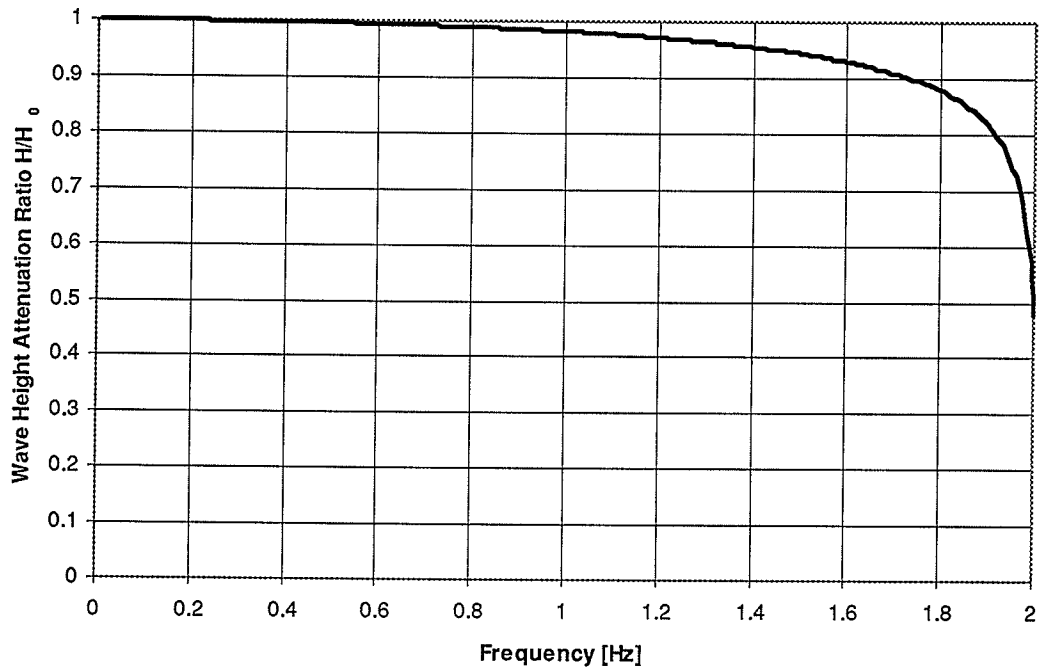


Figure 4.5b Ratio of wave height at probe location to wave height at waveboard as a function of wave frequency.

and Δ_{gap} is the average gap around the perimeter of the waveboard, in metres. With an average gap of 9.5 mm, the attenuation is most pronounced in the low frequency region of the spectrum as seen in Figure 4.6. This gap will clearly have ramifications for the accurate reproduction of long waves.

4.2.3. Wave Reflection

Wave energy generated by the oscillating waveboard is dissipated as heat and sound in the wave shoaling and breaking processes. While this is quite an effective mechanism of energy dissipation for short waves, long wave energy tends to be reflected back in the direction of the waveboard without breaking and with little attenuation. A random wavetrain based on a fully developed, idealized TMA spectrum, 600 seconds long initially sampled at 4 Hz, with a peak period of 2 seconds was sent to the waveboard. This wavetrain was fully corrected for spurious long and short second-order wave effects. To illustrate the effects of reflection on the recorded wave heights, the series was recycled 3 times during the course of a run. Coincident segments of the run during the first, second, and third time through the series are shown in Figure 4.7. Clearly, the records are very similar. Cycle 1 is uncorrupted by reflection since it shows the first pass through the series and looks cleaner than the other two. Cycles 2 and 3 are nearly identical which implies that the reflection effects are very small. Larger effects would tend to compound resulting in cycle 3 being significantly more corrupted than cycle 2. This figure also highlights the repeatability of the waveboard motion. All three cycles clearly stem from the same basic waveboard oscillations. It is only in the finest details of the waves that the records differ. Reflection coefficients were calculated over the generating range of 0 Hz to 2 Hz using a phase shift technique. Knowing the water surface elevation at wave probe WP1, the

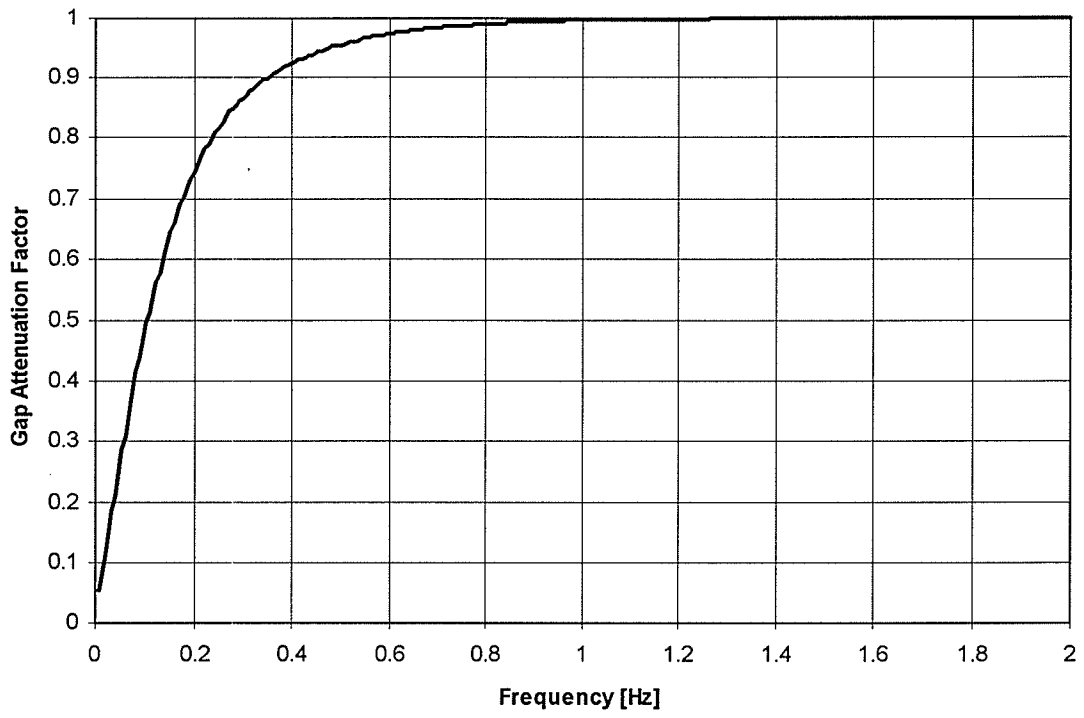


Figure 4.6 Wave height attenuation factor due to gap around waveboard

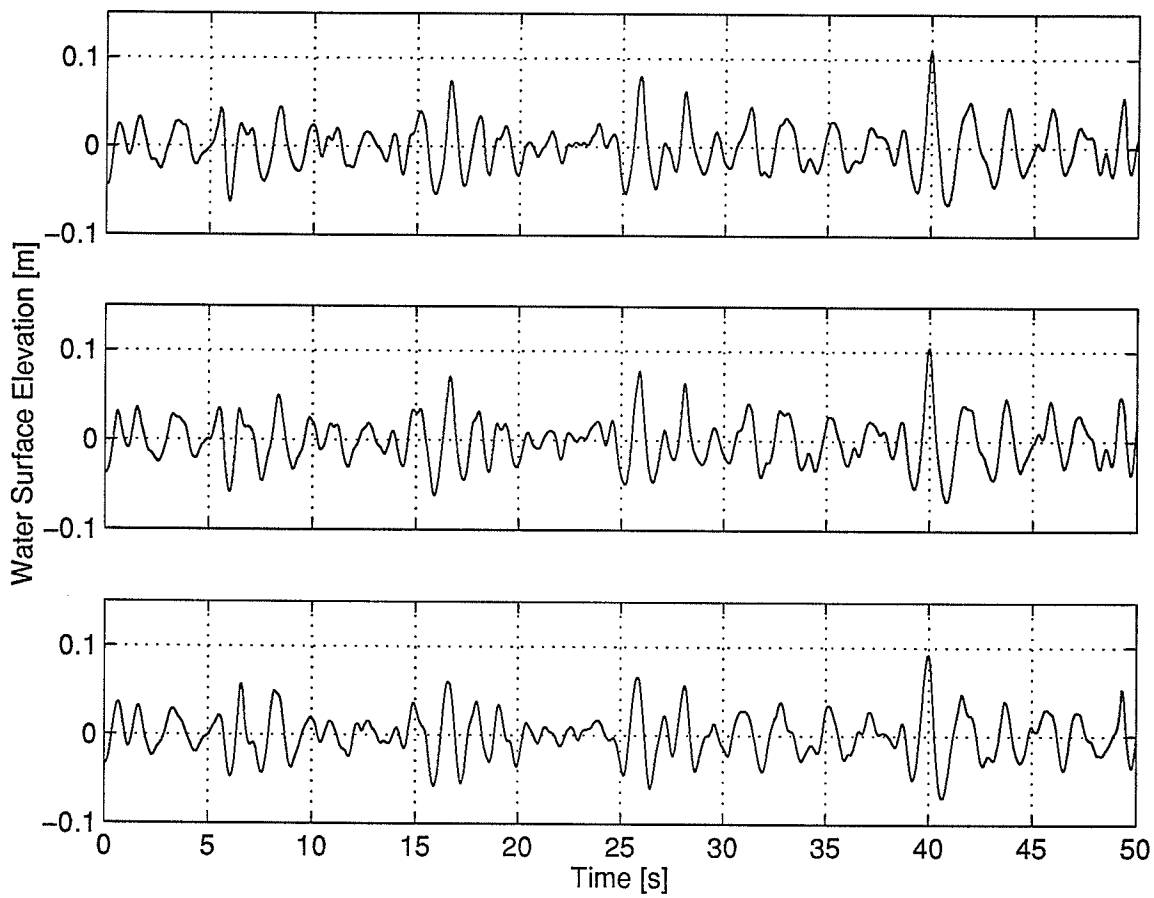


Figure 4.7 Effect of reflection on primary waves generated by a fully developed TMA spectrum, 1 m water depth, sampled at 4 Hz, $f_p = 0.5$ Hz..

expected wave height at probe WP2 can be calculated by assuming linear dispersion and applying a phase shift over the separation distance between the probes. Any difference between the calculated water surface elevation and the actual recorded water surface elevation is assumed to be a result of reflected wave energy. Reflection coefficients calculated on the random wavetrain in Figure 4.7 ranged from 86.6% at 0.121 Hz to 13.2% at 0.609 Hz. Reflection of long waves can be minimized by having the waves break gently over a distance by spilling rather than by suddenly and abruptly plunging (Ottesen Hansen *et al.*, 1980).

Chapter 5: Bispectral Analysis

The bispectrum was first introduced by Hasselmann *et al.* (1963) and was used to examine the skewness of two surface wave records collected off the coast of California. Since then bispectral techniques have been used to study nonlinearities in a wide variety of fields including earth noise (Haubrich, 1965), plasma fluctuations (Kim and Powers, 1979), and shoaling surface gravity waves (Elgar and Guza, 1985; Doering and Bowen, 1987).

If $\zeta(t)$ is a stationary random function of time, it can be represented as a superposition of statistically uncorrelated waves (*i.e.* having random phases). The “power” spectrum approach completely describes, to a first approximation, a Gaussian time series as

$$P(f) = \int_{-\infty}^{+\infty} R(\tau) e^{-i2\pi f\tau} d\tau, \quad (5.1a)$$

where

$$R(\tau) = E[\zeta(t)\zeta(t+\tau)], \quad (5.1b)$$

τ is a lag and $E[\]$ indicates an expected value. If the phase of the Fourier components are not randomly distributed but have a phase persistence, then the time series is not Gaussian. Unfortunately, the “power” spectrum is unable to detect deviations from a Gaussian form since it discards phase information. Deviations from a Gaussian form can be detected using the bispectrum. The bispectrum is formally defined as the Fourier transform of the second-order covariance function (Hasselmann *et al.*, 1963)

$$B(f_1, f_2) = \int_{-\infty}^{+\infty} \int_{-\infty}^{+\infty} S(\tau_1, \tau_2) e^{-i(2\pi(f_1\tau_1 + f_2\tau_2))} d\tau_1 d\tau_2 \quad (5.2a)$$

where

$$S(\tau_1, \tau_2) = E[\zeta(t) \zeta(t + \tau_1) \zeta(t + \tau_2)]. \quad (5.2b)$$

For digital data (*i.e.*, Fourier coefficients), the bispectrum can be expressed as (Haubrich, 1965; Kim and Powers, 1979)

$$B(f_1, f_2) = E[A(f_1)A(f_2)A^*(f_3)], \quad (5.3)$$

with the convention that $f_1 + f_2 = f_3$, $A(f)$ is the complex Fourier coefficient for frequency f , and $*$ denotes the complex conjugate. It can be shown that $B(f_1, f_2)$ will be zero unless waves are present at frequencies f_1 , f_2 , and f_3 , and there is a phase relation between the waves at these frequencies. Physically, if the waves present at f_1 , f_2 , and f_3 are normally excited modes, then each wave will be characterized by a statistically independent (random) phase and the expected value of $B(f_1, f_2)$ will be zero. However, if the sum or difference wave, f_3 , is generated through an interaction between f_1 and f_2 , then a phase coherence will exist and the expected value of $B(f_1, f_2)$ will be non-zero.

The bispectrum of a finite length record of a truly Gaussian process is non-zero because of the effects of the finite length. To distinguish normal independent modes from phase-coupled modes, it is convenient to express the bispectrum in a normalized form known as the bicoherence. Kim and Powers (1979) defined the bicoherence as

$$b^2(f_1, f_2) = \frac{|B(f_1, f_2)|^2}{E[|A(f_1)A(f_2)|^2]E[|A(f_3)|^2]} \quad (5.4)$$

$b^2(f_1, f_2)$ is normalized and is therefore independent of wave amplitude; $B(f_1, f_2)$ is not.

For large ν , where ν is the number of degrees of freedom, b^2 is expected to be χ^2 distributed (Haubrich, 1965). The 95% confidence limit on zero bicoherence is given by

$$b_{95\%}^2 = \frac{5.991}{\nu} \quad (5.5)$$

Finally, the bispectrum can also be expressed in terms of a biamplitude and biphas

$$B(f_1, f_2) = |B(f_1, f_2)|^{-i\beta(f_1, f_2)} \quad (5.6)$$

where the biphas $\beta(f_1, f_2)$ is given by

$$\beta(f_1, f_2) = \tan^{-1} \left\{ \frac{\Im[B(f_1, f_2)]}{\Re[B(f_1, f_2)]} \right\} \quad (5.7)$$

The bispectrum is used here to investigate the performance of the second-order correction algorithms using laboratory data collected in the HRTF random wave flume.

While the ultimate goal is to use the software developed for studying the numerous effects of random waves, to test the algorithms we start with the simplest case. Regular waves make the analysis tractable while still pointing out any problems with the computer code, yet by superposition they are the foundational components of a random wave train. The ability of the long wave and short wave corrections to eliminate spurious wave coupling

was tested using a bichromatic wave group with distinct sum and difference frequency components. The two corrections were tested exclusive of one another and jointly to examine any interference between the two cases. A grouped wave series was also generated without correction to establish a base case for comparison.

The wave series were generated to last 600 seconds (10 minutes) sampled at 4 Hz to give the series a 2 Hz Nyquist frequency. The grouped wave series were created with component frequencies of 0.33 and 0.38 Hz, both with amplitudes of 0.06 m. The resulting wavetrain was chosen because it has sufficient amplitude and sum/difference frequencies that the long and short wave corrections are clearly distinguishable. Long wave corrections were performed with a threshold value of 5%, short wave corrections with a value of 10%. For a bichromatic series these corrections are equivalent to full corrections.

The following notes are applicable to all the three-dimensional bispectral plots in this section:

- i) The origin is located at the left corner.
- ii) The two axes defining the frequency plane both run from 0 to 5 Hz.
- iii) A peak located in the bifrequency plane at frequencies f_1 and f_2 implicitly represents a triad; that is, the convention is, by definition, $f_1 + f_2 \rightarrow f_3$, where $f_3 = f_1 + f_2$.
- iv) There is symmetry about the line $f_1 = f_2$ since $f_1 + f_2 \rightarrow f_3$ is equivalent to $f_2 + f_1 \rightarrow f_3$.

Figures 5.1 to 5.4 show the biamplitude and bicoherence spectra for the bichromatic tests. The results for the uncorrected (base case) is shown in Figure 5.1. Three peaks are observed in the biamplitude spectrum. The largest peak centred at (0.39, 0.31) indicates a sum interaction between the two bichromatic components. The peaks centred at (0.70, 0.39) and (0.39, 0.08) indicate sum and difference interactions, respectively, between bichromatic and harmonic components. The faint distortion at (1.02, 0.31) suggests the initiation of interactions between the bichromatic components and higher sum components (*i.e.*, forced harmonics). While the biamplitude spectrum indicates the relative importance (*i.e.*, contribution to nonlinear properties) of triads in the wave field, it does not identify significantly coupled interactions in regions of low spectral amplitude; the bicoherence spectrum does.

For a bichromatic process it has been shown (Kim and Powers, 1979) that $b^2(f_1, f_2)$ represents the fraction of power at f_3 that results from nonlinear coupling between f_1 and f_2 . For example, if $b^2(f_1, f_2) = 1$ then the power at f_3 is due entirely to coupling between components f_1 and f_2 . Conversely, if $b^2(f_1, f_2) = 0$, then f_3 is a normal independent mode of the system and the power at f_3 is not the result of coupling between f_1 and f_2 . Unfortunately, there are two possible directions of energy flow, *i.e.*, $f_1 + f_2 \rightarrow f_3$ and $f_1 - f_2 \rightarrow f_3$, consequently, the bispectrum cannot be used to determine the direction of energy flow.

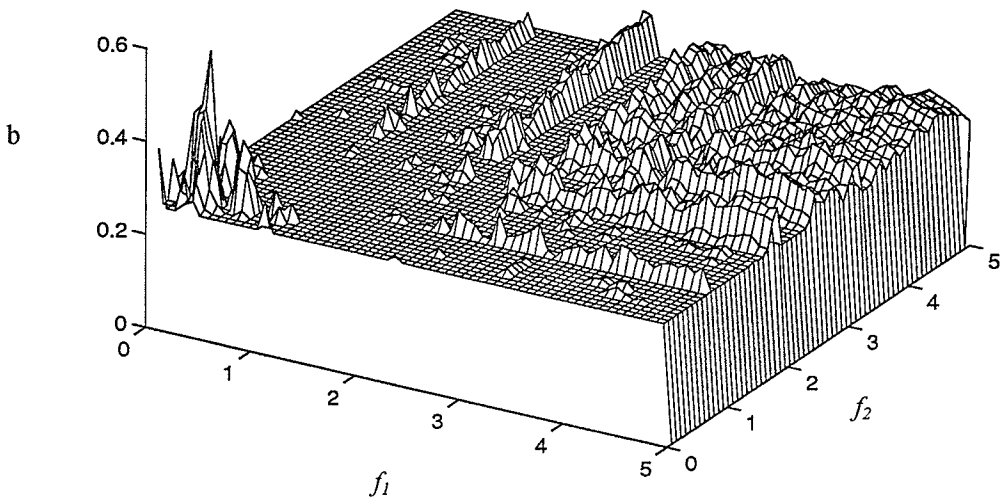
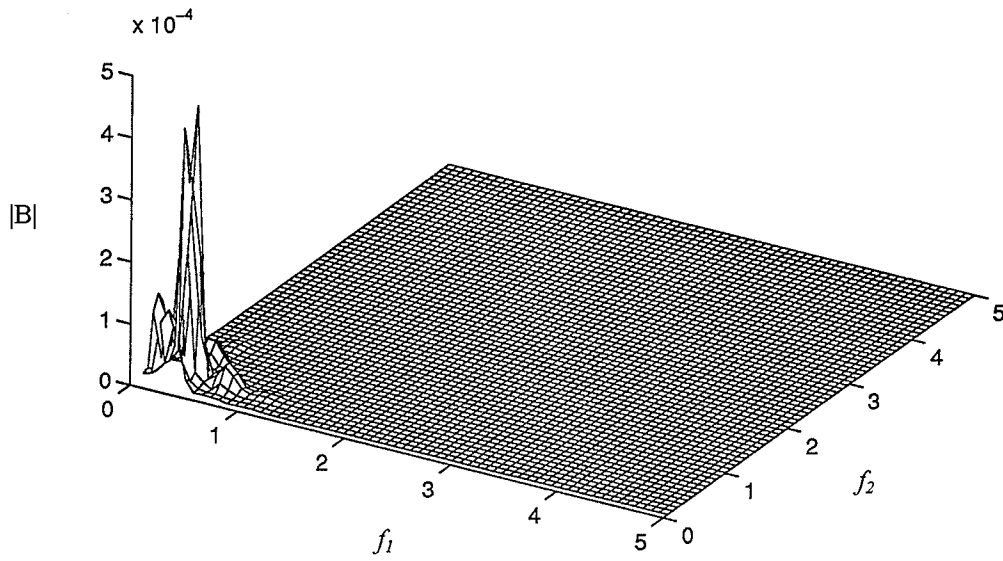


Figure 5.1 Bi-amplitude and bicoherence spectra for bichromatic wave series ($f_m = 0.31$ Hz, $f_n = 0.39$ Hz) with no corrections. $\delta f = 0.0781$ Hz, $\nu = 92$ d.o.f.

Figure 5.1 also shows the bicoherence spectrum for the base case. The normalized strength of the nonlinear interactions observed in the bi-amplitude spectrum are now apparent. The interaction between the two fundamental bichromatic frequencies is quite strong ($b^2(0.39, 0.31) \approx 0.70$) and well above the 95% confidence limit for zero bicoherence ($= 0.26$) which is given by the thickness of the “slab”. The “noise” observed above 1 Hz is believed to be an artifact of the mechanical generation process.

Figure 5.2 shows the bi-amplitude and bicoherence spectra for the long wave corrected record. Since the bichromatic record consists of two similar frequencies, wave groupiness results. The (temporal) variation in wave height gives rise to gradients in radiation stress (Longuet-Higgins and Stewart, 1964) and hence the presence of a wave at the difference frequency ($f_1 - f_2 \rightarrow \Delta f$). During the mechanical generation process, the negative velocity associated with this long wave is reflected from the waveboard and cancels out the natural long wave. The long wave correction adds back this canceled wave. While the bicoherence peaks associated with difference interactions are “cleaned up”, the strength of these interactions is diminished. This suggests a possible shortcoming in the long wave correction theory and/or problems arising from the gap around the perimeter of the waveboard.

Figure 5.3 shows the results for the short wave corrected record. The strength of the sum interaction at (0.39, 0.31), which is the only short wave correction that occurs for a bichromatic record has been increased appreciably; this is in keeping with theoretical

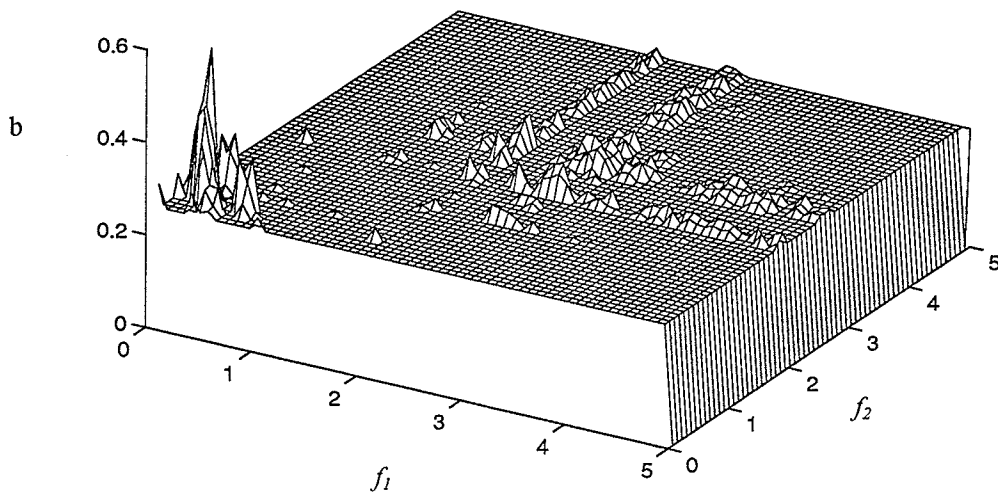
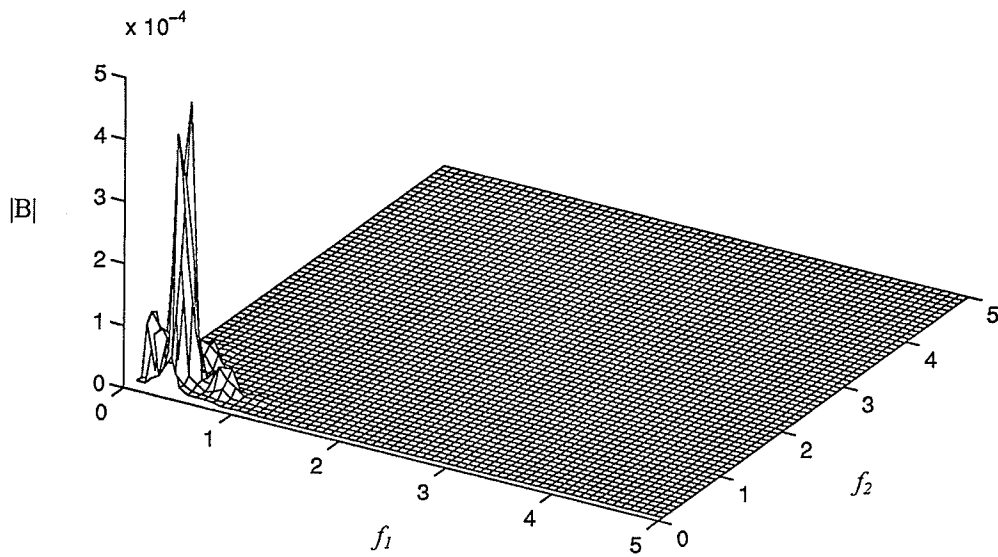


Figure 5.2 Biamplitude and bicoherence spectra for bichromatic wave series ($f_m = 0.31$ Hz, $f_n = 0.39$ Hz) with long wave corrections only. $\delta f = 0.0781$ Hz, $\nu = 92$ d.o.f.

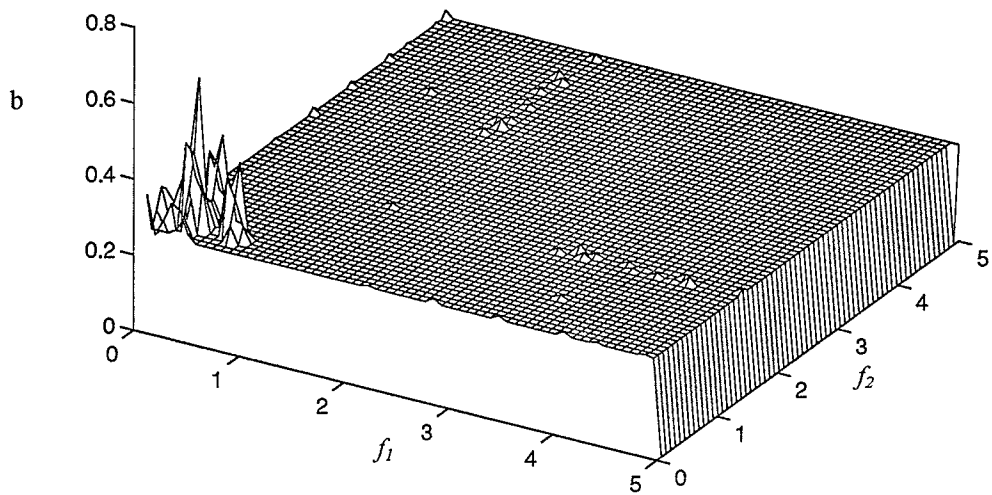
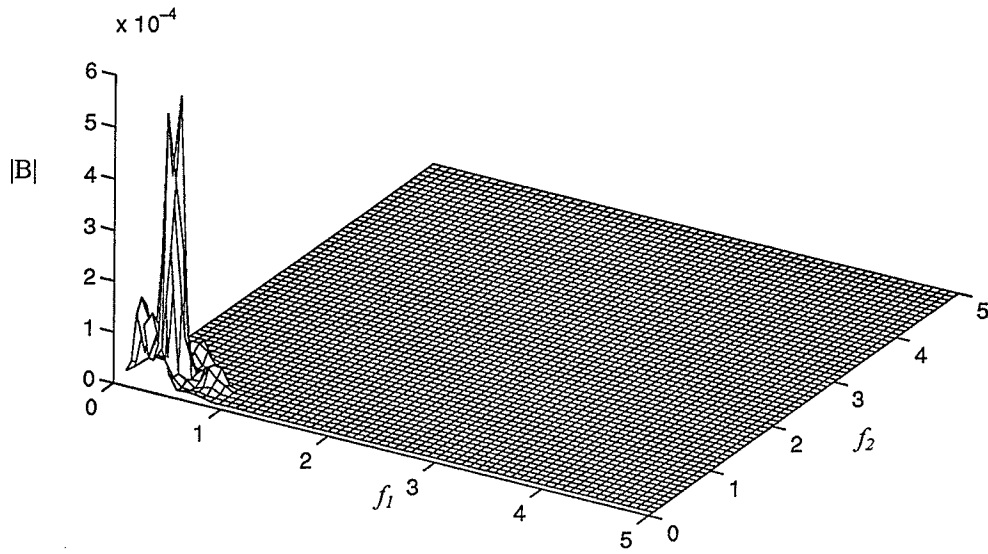


Figure 5.3 Biamplitude and bicoherence spectra for bichromatic wave series ($f_m = 0.31$ Hz, $f_n = 0.39$ Hz) with short wave corrections only. $\delta f = 0.0781$ Hz, $\nu = 92$ d.o.f.

expectations as spurious free short wave components that diminish coupling have been reduced and hopefully eliminated. Any change in the amplitude of the peak at (0.70, 0.31) is a second-order effect resulting from changes in spectral components at 0.70 Hz, the sum frequency ($0.39 + 0.31 \rightarrow 0.70$). It is interesting to note that high frequency coupling amongst frequencies greater than 1 Hz is significantly reduced when either the long wave or short wave correction is employed. The reason for this is not clear. The presence of coupling at such high frequencies has been observed in another flume (Doering, personal communication).

Figure 5.4 shows the bispectral results when both the long and short wave correction are employed. The combined correction leads to two well-defined sum and difference interaction peaks located at (0.39, 0.31) and (0.39, 0.08), respectively.

Finally, a random wavetrain was analyzed both in uncorrected and fully corrected forms to show the extension of the theory to the usual case of "natural" waves. The wave records were 600 seconds in length, sampled at 4 Hz, based on a fully developed, TMA spectrum, with a peak frequency of 0.5 Hz. The wave statistics are the same as those found in the wave records that were analyzed numerically in chapter 3. The bispectral results for an uncorrected and fully corrected random wave train are shown in Figures 5.5 and 5.6, respectively. The biamplitude spectra show an increase in the strength of both the sum and difference interactions occurring within the spectral peak. The bicoherence spectra of a broad banded process are not readily interpreted.

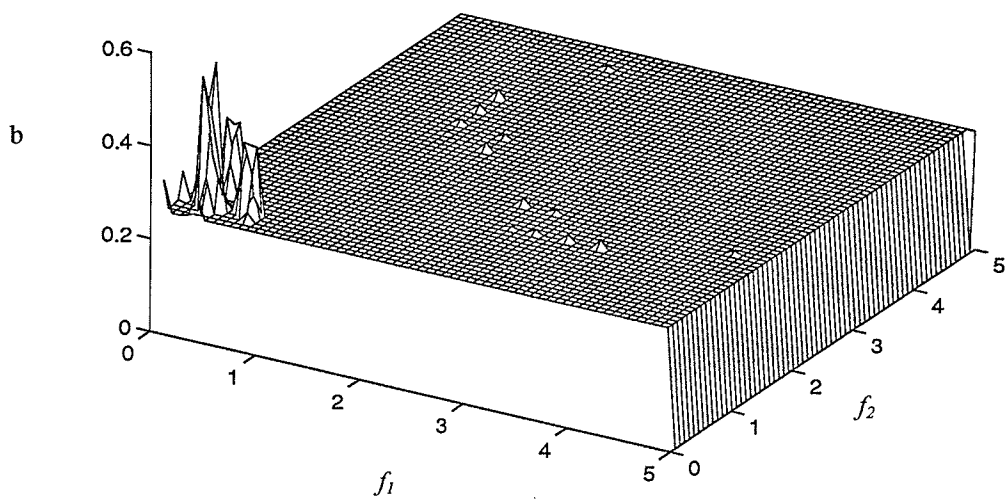
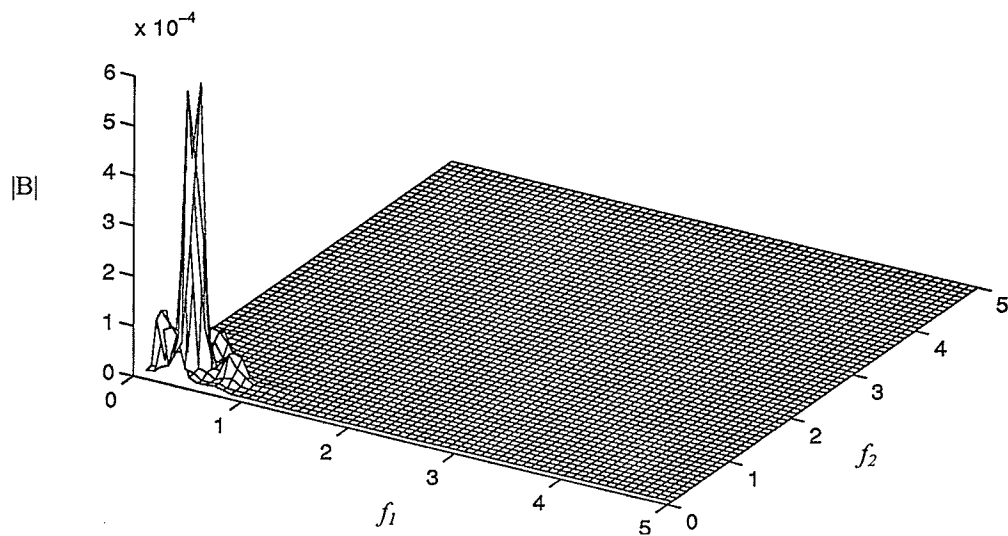


Figure 5.4 Biamplitude and bicoherence spectra for bichromatic wave series ($f_m = 0.31$ Hz, $f_n = 0.39$ Hz) with full corrections. $\delta f = 0.0781$ Hz, $\nu = 92$ d.o.f.

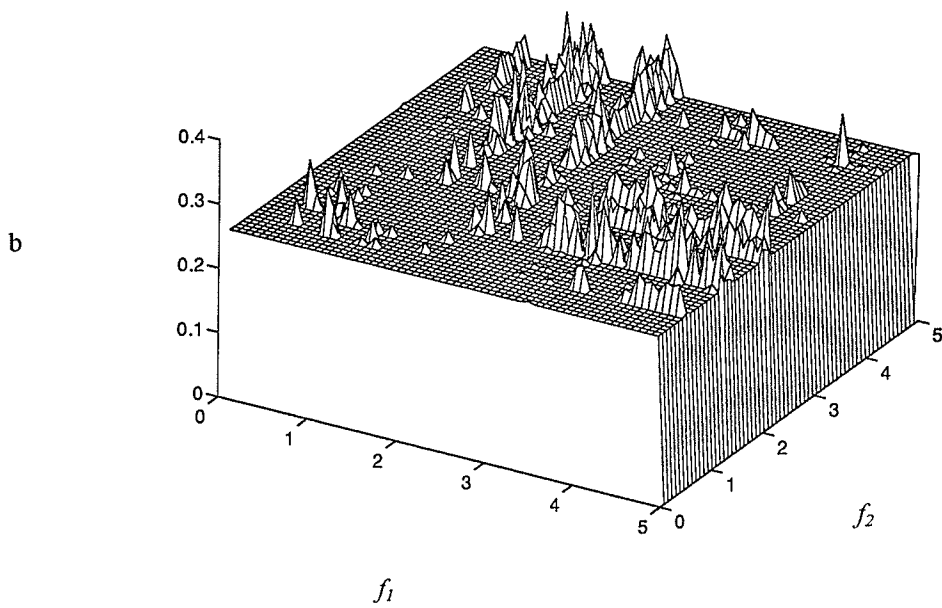
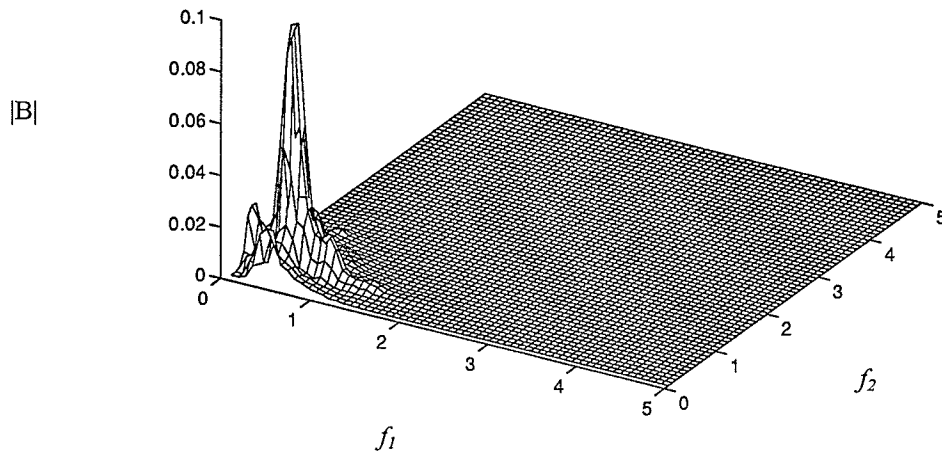


Figure 5.5 Biamplitude and bicoherence spectra for random wave series (fully developed TMA spectrum, 1 m water depth, sampled at 4 Hz, $f_p = 0.5$ Hz) with no corrections. $\delta f = 0.0781$ Hz, $\nu = 90$ d.o.f.

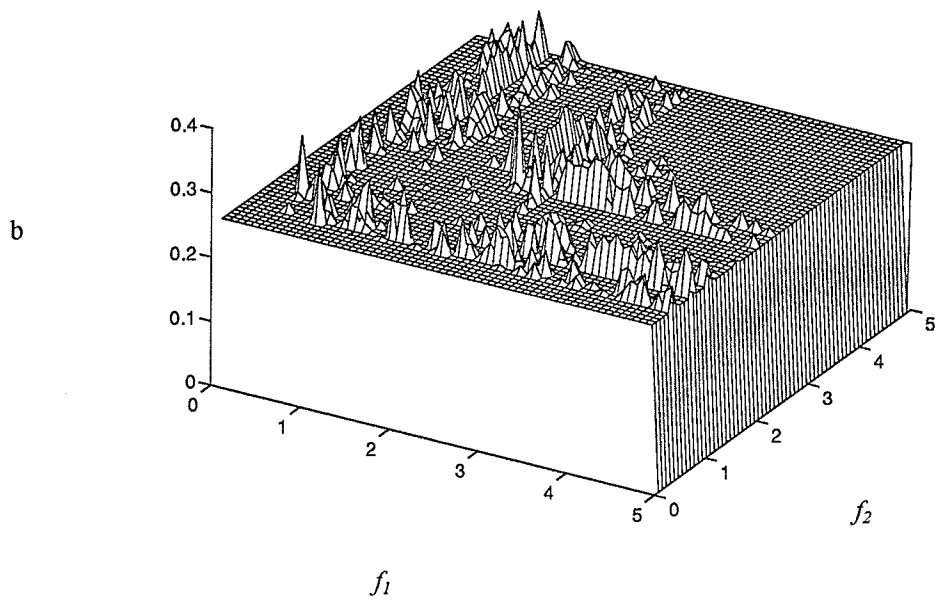
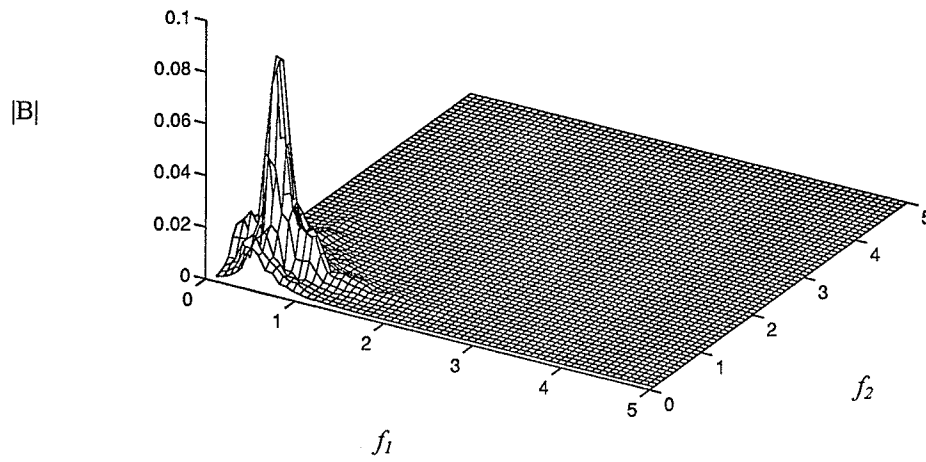


Figure 5.6 Biampitude and bicoherence spectra for random wave series (fully developed TMA spectrum, 1 m water depth, sampled at 4 Hz, $f_p = 0.5$ Hz) with full corrections. $\delta f = 0.0781$ Hz, $\nu = 90$ d.o.f.

Chapter 6: Conclusions and Recommendations

6.1. Summary and Conclusions.

For the extrapolation of laboratory data to full scale sea conditions it is essential to have a realistic reproduction of the sea in laboratory experiments. Since it is impractical and difficult to generate sufficiently large waves in a flume using nature's mechanism (*i.e.*, wind) waveboards are used. However, the mechanical generation of realistic waves is quite complex. The movement of the waveboard and the boundary condition at the waveboard give rise to numerous unwanted second-order effects that can seriously corrupt or interfere with natural phenomena. In a natural wave train, with the spectral energy concentrated around the peak frequency, the non-linearity of the free-surface boundary conditions introduces sub- and superharmonics which are phase locked to the primary wave components.

The subharmonics (or bound long waves) can generate the forcing for long period harbour oscillations, slow-drift motions of moored vessels and tension-leg platforms, and offshore sand-bar formation due to sediment transport. The superharmonics introduce sharper-peaked crests and flatter troughs, that are important for sediment transport due to wave asymmetry and can be of importance for forces on offshore structures. An incorrect (linear) reproduction in the laboratory generates free waves at the same frequencies as the bound sub- and superharmonics, but travelling at a different speed. This difference in speed between the free and bound wave components results in spatial variations in the water surface fluctuations.

Solutions to mechanically produce waves, correct to second-order, have been proposed by Sand (1982), Barthel *et al.* (1983), and Sand and Mansard (1986a,b). They introduced second-order transfer functions that calculate the amplitude of the spurious, free, second-order waves created by using a first-order driving signal. These second-order waves are subtracted out of the first-order control signal resulting in a driving signal free of spurious second-order effects. These algorithms were developed into MATLAB-based code to yield an interactive package to generate a first-order wave train using the parameters input by the user and to calculate second-order long and short wave corrections to eliminate the spurious free waves that are inherent in the mechanical generation process.

The complexity of the second-order correction algorithms leads to lengthy computation times that increase proportional to n_f^2 where n_f is the number of frequencies used to make a "random" wavetrain. To make the algorithms more efficient a method was developed to limit the number of frequencies used in the second-order corrections using a thresholding technique outlined in section 3.3. The long wave threshold limits the corrections to only those frequency differences that constitute the long wave portion of the spectrum. As the numerical simulation results clearly indicate, the threshold limit can be set as low as 5% without significantly altering the amplitude or the appearance of the correction. The application of thresholding to the short wave correction limits the computation to frequencies that are a result of an interaction of two frequencies that lie near the spectral peak. The application of high threshold limits significantly lowers the short wave amplitude and changes the appearance of the corrections. However, a threshold on the

order of 30% reduces the computational effort by about a factor of two without drastically changing the short wave correction series.

Laboratory testing of the WAVGEN wave generation software was undertaken in the Hydraulics Research & Testing Facility. The use of a laboratory setting introduces several limitations to the wave generation process that can affect the quality of the data collected. The ability of the waveboard to respond to a control signal, wave attenuation due to sidewall and bottom friction, wave attenuation due to an imperfect seal around the waveboard and reflection of the incident waves off the end of the flume are all factors that have been considered.

The response of the waveboard to a control signal was considered to be exceptional. Using an analog function generator, a low amplitude sine function was sent to the waveboard at frequencies starting at 0.1 Hz and progressing up to 5 Hz. These tests failed to produce any noticeable deterioration in the waveboard's ability to reproduce the control signal.

Wave attenuation due to bottom friction is common to both the laboratory setting and the natural setting. Friction from the sidewalls of the flume, found only in the laboratory, significantly affected only the highest frequency wave components. The amplitude of waves at these high frequencies at the waveboard is typically on the order of millimetres making the effects of frictional attenuation negligible. Any gap around the edges of a waveboard results in the attenuation of waves as the water flows through the gap,

impinges on the waveboard, and generates a spurious free wave. With an average gap of 9.5 mm, the attenuation constant was significant at low, long wave frequencies.

In a natural setting, wave energy reflected off of the shoreline propagates offshore and is of little consequence. With the solid planar waveboard boundary found in a wave flume, reflection is a much larger problem. Long wave energy can propagate back and forth between the end wall of the flume and the waveboard setting up a standing wave pattern. Reflection of wave energy off the end wall of the flume was calculated to be anywhere from 86.6% to 16.2% depending on the frequency of the incident waves. The use of a rather simplistic approach to calculating these reflection coefficients may be the reason for these high results. The traces of the wave records presented do not apparently exhibit such a high degree of reflection.

Bispectral testing of the second-order correction algorithms is a new approach to determining whether the algorithms do in fact eliminate spurious free waves. Previous investigators examined the stability of the waveforms over the length of the flume and the amplitude of the power spectrum in the long and short wave frequency bands as a means of verifying their algorithms. These methods did not take into account the changes in the strength of the phase coupling between the bound second-order waves and the primary waves brought about by the presence of free waves at the bound wave frequencies. Bispectral testing of bichromatic wave trains clearly indicate that the correction algorithms eliminate both the spurious wave amplitude and the effects of the spurious waves on phase coupling as seen by comparing the results for an uncorrected wavetrain with the results for

a fully corrected wavetrain. Testing of a random wave series showed similar results for the biamplitude spectrum. The implication of the bicoherence spectra of a broad banded process are not so clear.

6.2. Recommendations for Future Work.

For a substantial simplification of the long wave correction theory, the evanescent modes can be ignored when the waveboard motion makes a good fit to the velocity profile of the desired progressive waves. Situations where this approximation fails are often encountered. Schäffer (1994) quantified the error introduced by ignoring the effects of evanescent modes in second-order wave generation. Schäffer (1996) recently presented the complete second-order wavemaker theory for irregular waves. A complex representation was chosen to facilitate and simplify the theoretical calculations. The theory was verified for a piston-type wavemaker using regular waves, wave groups, and irregular waves. This algorithm should be coded and included as an option for the user to select in WAVGEN and possibly could be the only second-order correction option available.

The WAVGEN software would benefit from incorporating a graphical user interface (GUI) to make it more user friendly. The user would be able to immediately see the results of changing the wave parameters or groupiness factor on the primary wave train and continue on to the corrections and paddle control signal generation once satisfied with the form of the primary waves. A GUI would also make it possible for the user to correct input errors without restarting WAVGEN each time. Limits on the input parameters

could be more clearly defined by the use of a slider bar between the upper and lower bounds as the input mechanism.

Based on the calculated attenuation constant due to the gap around the waveboard and the results of the bispectral testing of the long wave corrected wave record, it would be beneficial to retest the long wave algorithm after sealing the gap around waveboard. This would be a better solution than simply overdriving the lower frequency components of the spectrum. Overdriving leads to large waveboard excursions that can not always be accommodated by the 1 metre piston stroke of the HRTF wave generator.

Once the gap around the waveboard is sealed a program of rigorous testing of the algorithms using the bispectrum and bichromatic waves should be carried out. Results for bichromatic series with a wide range of f_m and f_n values and the corresponding range of bound long and short waves should be examined. Deep, intermediate, and shallow water primary waves should be examined to see the effects of the corrections when different spurious wave phenomena are dominant. This sort of exhaustive testing would serve to increase the confidence in the algorithms and in the WAVGEN code based on those algorithms.

References

- Barthel, V., Mansard, E.D.P., Sand, S.E., and Vis, F.C. 1983. Group bounded long waves in physical models. *Ocean Engrg.* **10**(4), 261-294.
- Baryla, A. J. 1996. On the mechanical generation of realistic waves. B. Sc. Thesis. University of Manitoba.
- Biéssel, F. 1951. Etude théorique d'un type d'appareil à houle. *La Houille Blanche* **6**(2), 152-165.
- Bouws, E., Günther, H., Rosenthal, W., and Vincent, C. L. 1985. Similarity of the wind wave spectrum in finite depth water. *J. Geophys. Res.* **90**(C1), 975-986.
- Buhr Hansen, J., Schiolten, P., and Svendsen, I. A. 1975. Laboratory generation of waves of constant form. Series Paper **9**, Inst. of Hydrodyn. and Hydraulic Engrg. (ISVA), Tech. Univ. of Denmark, 56 pp.
- Dean, R. G., and Sharma, J. N. 1981. Simulation of wave systems due to non-linear directional spectra. *Proc. Int. Symp. Hydrodynamics in Ocean Engrg., The Norwegian Inst. of Techn.* **2**, 1211-1222.
- Doering, J. C., and Bowen, A. J. 1987. Skewness in the nearshore zone: A comparison of estimates from Marsh-McBirney current meters and colocated pressure sensors. *J. Geophys. Res.* **92**, 13, 173 - 183.
- Donelan, M. A., Hamilton, J., Hui, W. H. 1985. Directional spectra of wind generated waves. *Philos. Trans. R. Soc. Lond.* **A315**, 509-562.
- Elgar, S. L., and Guza, R. T. 1985. Observations of bispectra of shoaling surface gravity waves. *J. Fluid Mech.* **161**, 425-448.
- Flick, R. E., and Guza, R. T. 1980. Paddle generated waves in laboratory channels. *J. Watways, Port, Coastal Ocean Div., ASCE* **106**(WW1), 79-97.
- Fontanet, P. 1961. Théorie de la génération de la houle cylindrique par un batteur plan. *La Houille Blanche* **16**(1), 3-31 (part 1) and 174-196 (part 2).
- Funke, R. E. and Mansard, E. D. P. 1979. On the synthesis of realistic sea states in a laboratory flume. National Research Council of Canada, Hydraulics Laboratory Tech. Rep. LTR-HY-66.

- Hasselmann, K., Munk, W., and MacDonald, G. 1963. Bispectra of ocean waves in *Time Series Analysis* (edited by M. Rosenblatt). New York : Wiley, 125-139.
- Hasselmann, K., *et al.* 1973. Measurements of wind-wave growth and swell decay during the Joint North Sea Wave Project (JONSWAP). *Dt. hydrogr. Z.* **12**, 9-95.
- Haubrich, R. A. 1965. Earth noises, 5 to 500 millicycles per second. *J. Geophys. Res.* **70**, 1415-1427.
- Hudspeth, R. T. and Sulisz, W. 1991. Stokes drift in two-dimensional wave flumes. *J. Fluid Mech.* **230**, 209-229.
- Hunt, J. N. 1952. Viscous damping of waves over an inclined bed in a channel of finite width. *La Houille Blanche*, 836-842.
- Jamieson, W. W. and Mansard, E. D. P. 1987. An efficient upright wave absorber. *Proc. Specialty Conf. on Coastal Hydrodynamics*, ASCE.
- Kim, Y. C. and Powers, E. J. 1979. Digital bispectral analysis and its applications to non-linear wave interactions. *IEEE Trans. on Plasma Sc.* **1**, 120-131.
- Klopman, G. and Van Leeuwen, P. J. 1990. An efficient method for the reproduction of non-linear random waves. *Proc. 22nd Int. Conf. Coastal Engrg.*, Delft, The Netherlands, 1990, ASCE, New York, **1**, 478-488.
- Longuet-Higgins, M. S., and Stewart, R. W. 1962. Radiation stress and mass transport in gravity waves with application to surf beat. *J. Fluid Mech.* **13**, 481.
- Longuet-Higgins, M. S., and Stewart, R. W. 1964. Radiation stresses in water waves: a physical discussion with applications. *Deep Sea Res.* **11**, 529-562.
- Madsen, O. S. 1971. On the generation of long waves. *J. Geophys. Res.* **76**, 8672-8683.
- Moubayed, W. I. and Williams, A. N. 1994. Second-order bichromatic waves produced by a generic planar wavemaker in a two-dimensional flume. *J. Fluids and Structures* **8**, 73-92.
- Ottesen Hansen, N.-E. 1978. Long period waves in natural wave trains. *Prog. Rep.* **46**, Inst. of Hydrodyn. and Hydraulic Engrg. (ISVA), Tech. Univ. of Denmark, 13-24.
- Ottesen Hansen, N.-E., Sand, S. E., Lundgren, H., Sorensen, T., and Gravesen, H. 1980. Correct reproduction of group-induced long waves. *Proc. Seventeenth Coastal Engineering Conf.*, ASCE.

- Sand, S. E. 1982. Long wave problems in laboratory models. *J. Watways, Port, Coastal Ocean Div., ASCE* **108**(WW4), 492-503.
- Sand, S. E. and Donslund, B. 1985. Influence of wave board type on bounded long waves. *J. Hydraulic Res.* **23**(2), 147-163.
- Sand, S. E. and Mansard, E. D. P. 1986a. Description and reproduction of higher harmonic waves. National Research Council of Canada, Hydraulics Laboratory Tech. Rep. TR-HY-012.
- Sand, S. E. and Mansard, E. D. P. 1986b. Reproduction of higher harmonics in irregular waves. *Ocean Engrg.* **13**(1), 57-83.
- Schäffer, H. A. 1993. Second-order irregular wave generation in flumes - Computation of transfer function by an asymptotic summation method. Proc. *Waves '93: 2nd Int. Symp. Ocean Wave Measurement and Analysis*, New Orleans, LA, USA.
- Schäffer, H. A. 1994. The influence of evanescent modes in second-order wave generation. Proc. *Waves - Physical and numerical modelling*, Vancouver, BC, Canada.
- Schäffer, H. A. 1996. Second order wavemaker theory for irregular waves. *Ocean Engrg.* **23**(1), 47-88.
- Stokes, G. G. 1847. On the theory of oscillatory waves. *Trans. Camb. Phil. Soc.* **8**, 441-455.
- Sulisz, W. and Hudspeth, R. T. 1993. Complete second-order solution for water waves generated in wave flumes. *J. Fluid Struct.* **7**(3), 256-268.
- Treloar, P. D. and Brebner, A. 1970. Energy losses under wave action. Proc. *12th Conf. Coastal Eng.*, Washington, D.C., 257-267.